INNOVATIVE POLYHYDROXYALKANOATES/PEROVSKITE/ SURFACTANT COMPOSITE FILM AS AN ECO-FRIENDLY PROTON EXCHANGE MEMBRANE FOR WATER FILTRATION

NUR AMIRAH BINTI MOHD FAIZAL

FACULTY OF SCIENCE
UNIVERSITI MALAYA
KUALA LUMPUR

2024

INNOVATIVE POLYHYDROXYALKANOATES/PEROVSKITE/ SURFACTANT COMPOSITE FILM AS AN ECO-FRIENDLY PROTON EXCHANGE MEMBRANE FOR WATER FILTRATION

NUR AMIRAH BINTI MOHD FAIZAL

DISSERTATION SUBMITTED IN FULFILMENT OF THE REQUIREMENTS FOR THE DEGREE OF MASTER OF SCIENCE

INSTITUTE OF BIOLOGICAL SCIENCES
FACULTY OF SCIENCE
UNIVERSITI MALAYA
KUALA LUMPUR

2024

UNIVERSITI MALAYA

ORIGINAL LITERARY WORK DECLARATION

Name of Candidate: **NUR AMIRAH BINTI MOHD FAIZAL**

Matric No: **S2151460/1**

Name of Degree: **MASTER OF SCIENCE**

Title of Thesis:

INNOVATIVE POLYHYDROXYALKANOATES/PEROVSKITE/ SURFACTANT COMPOSITE FILM AS AN ECO-FRIENDLY PROTON EXCHANGE MEMBRANE FOR WATER FILTRATION

Field of Study:

LIFE SCIENCE (BIOLOGY & BIOCHEMISTRY)

I do solemnly and sincerely declare that:
1) I am the sole author/writer of this Work;
2) This Work is original;
3) Any use of any work in which copyright exists was done by way of fair dealing and for permitted purposes and any excerpt or extract form, or reference to or reproduction of any copyright work has been disclosed expressly and sufficiently and the title of the Work and its authorship have been acknowledged in this Work;
4) I do not have any actual knowledge nor do I ought reasonably to know that the making of this work constitutes an infringement of any copyright work;
5) I hereby assign all and every rights in the copyright to this Work to the University of Malaya ("UM"), who henceforth shall be owner of the copyright in this Work and that any reproduction or use in any form or by any means whatsoever is prohibited without the written consent of UM having been first had and obtained;
6) I am fully aware if in the course of making this Work I have infringed any copyright whether intentionally or otherwise, I may be subject to legal action or any other action as may be determined by UM.

Candidate's Signature: Date:

Subscribed and solemnly declared before:

Witness Signature: Date:

Name:

Designation:

INNOVATIVE POLYHYDROXYALKANOATES/PEROVSKITE/ SURFACTANT COMPOSITE FILM AS AN ECO-FRIENDLY PROTON EXCHANGE MEMBRANE FOR WATER FILTRATION

ABSTRACT

The focus of this project is to analyse the potential of Polyhydroxyalkanoate-Perovskite-Tween 80 (PHA-PV-T80) composites as a selective proton exchange membrane (SPEM) for water filtration. PHA-PV-T80 composites were prepared by initially synthesizing PHA from *Pseudomonas putida* BET001 *via* a batch fermentation process; then PHA was blended with distinct concentrations of perovskite and Tween 80 ranging from 0.01 – 0.0025 % (*w/v*) and 1.5 – 4.5 % (*w/v*), respectively. Ultrasonication was used to enhance the mixing process. The sonicated solution was cast onto a petri dish to be air-dried until it reached a constant weight. Mcl-PHA monomer constituents were identified using GCMS and ^{1}H-NMR. The functional group changes, thermal properties, and surface morphology of PHA-PV-T80 composites were characterized using FTIR, TGA, and FESEM, respectively. Proton transport analysis was carried out to understand the efficiency of its transfer across the membrane surface by studying the flux ($mol.min^{-1}.cm^{-2}$) of each membrane. PHA-PV0.01%-T80 4.5% showed the highest flux among the investigated composites. Analysis of the apparent rate constant, *k'*, provided insights on the enhanced proton flux process in a specific membrane composite; compositing of surfactant with a larger hydrophilic head group in the PHA matrix, as opposed to increasing the perovskite amount, plays a greater role in the partitioning of water molecules on the membrane surface, hence facilitating proton flux.

Keywords: polymer nanocomposite, biological polymer, poly-3-hydroxyalkanote, proton permeability

FILEM KOMPOSIT MESRA ALAM POLIHIDROKSIALKANOAT/PEROVSKIT/SURFAKTAN SEBAGAI MEMBRAN PERTUKARAN PROTON UNTUK PENAPISAN AIR

ABSTRAK

Fokus projek ini adalah untuk menganalisis potensi komposit Polihidroksialkanoat-Perovskit-Tween 80 (PHA-PV-T80) sebagai membran yang selektif kepada pertukaran proton (SPEM) untuk aplikasi penapisan air. Komposit PHA-PV-T80 telah disediakan dengan mensintesis PHA daripada *Pseudomonas putida* BET001 melalui proses penapaian kelompok terlebih dahulu; kemudian PHA dicampurkan dengan perovskite dan Tween 80 yang berbeza nilai kepekatan antaranya, 0.01- 0.0025% (*w/v*) dan 1.5 – 4.5% (*w/v*). Teknik ultrasonik digunakan untuk meningkatkan kebolehcampuran larutan tersebut. Larutan yang telah sebati dituang pada piring petri untuk dikeringkan sehingga berat tetap dicapai. Monomer yang terdapat dalam struktur mcl-PHA telah dikenalpasti dengan menggunakan GCMS dan ^{1}H-NMR. Perubahan kumpulan fungsian, sifat terma dan morfologi permukaan komposit PHA-PV-T80 dicirikan menggunakan FTIR, TGA dan FESEM. Analisis proton telah dijalankan untuk memahami kecekapan pergerakan proton dalam membran dengan mengkaji nilai fluks (mol.min^{-1}.cm^{-2}) bagi setiap membran. PHA-PV0.01%-T80 4.5% menunjukkan nilai fluks tertinggi berbanding komposit yang lain dengan sisihan piawai < 5 %. Pengkajian nilai *k*', iaitu tetapan kadar jelas, telah memberikan gambaran tentang proses peningkatan fluks proton dalam setiap komposit membrane. Pencampuran surfaktan yang mempunyai kumpulan kepala hidrofilik lebih besar dalam matriks PHA, berbanding peningkatan kepekatan perovskit, memainkan peranan lebih besar dalam pembahagian molekul air pada permukaan membrane, justeru pergerakan proton dipermudahkan.

Kata kunci: Nanokomposite polimer, polimer biologi, poli-3-hidroksialkanoat, ketelapan proton

ACKNOWLEDGEMENTS

To start with, my deepest gratitude is given to my Creator the Almighty Allah SWT for enriching me with strength and composure during this journey of my master's degree.

A warm thank you to both my project supervisors, Professor Dr Mohammad Suffian bin Mohammad Annuar and Dr Khairul Anwar bin Ishak for all the support and encouragement they had given me during my research project. Without their guidance and constant feedback, my master's degree would not have been achievable. I am also grateful for their aid throughout the whole process of my master's degree. The knowledge and techniques taught to me by them were very useful as it had made me further sharpen my laboratory and theoretical knowledge.

Other than that, I truly appreciate all my close friends who were there with me through my up's and down. Their advice and prayers had eased the burden felt by me throughout this journey. Kindness and tolerance were two values I was blessed with by them in our friendship.

Furthermore, uttermost gratitude for both my parents for providing me with continuous support. The continuous challenges I faced to complete and collect my experimental data had put a tall on my mental health however my parents had always been there to lend a shoulder to cry on. The successful completion of my master's thesis is due to their love and motivation.

Finally, I extend my appreciation to Universiti Malaya for providing me with their financial support from the Fundamental Research Grant Scheme (FRGS), which made this research possible.

TABLE OF CONTENTS

LIST OF FIGURES

LIST OF TABLES

LIST OF SYMBOLS AND ABBREVIATIONS

α	:	alpha
k’	:	apparent rate constant
≈	:	approximate
β	:	beta
°	:	degree
°C	:	degree Celsius
°C min^{-1}	:	degree Celsius per minute
δ	:	delta
T_g	:	glass transition temperature
T_m	:	melting temperature
%	:	percentage
T_d	:	thermal degradation temperature
θ	:	theta
AAc	:	Acrylic acid
ATR	:	attenuated total reflectance
$BaCeO_3$	:	Barium cerate
$BaZrO_3$	:	Barium zirconate
C=O	:	carbonyl
$CaCl_2.2H_2O$	:	Calcium chloride dihydrate
$CaTiO_3$	:	Calcium titanium oxide
$CDCL_3$	:	Chloroform-d
CH_2	:	methylene
CH_3	:	methyl
cm	:	centimeter
cm^{-1}	:	wavenumber

CMC	:	Critical Micelle Concentration
CNT	:	Carbon Nanotubes
CO_2	:	Carbon dioxide
C-O-C	:	ether
$CoSO_4.7H_2O$	:	Cobalt (II) sulfate heptahydrate
$CuCl_2.2H_2O$	:	Copper (II) chloride dihydrate
$FeSO_4.7H_2O$	:	Iron (II) sulfate heptahydrate
g	:	gram
g L^{-1}	:	gram per Liter
H_2SO_4	:	Sulfuric acid
H_3O^+	:	hydronium ions
$H_5O_2^+$	:	Zundel cation
$H_9O_4^+$	:	Eigen cation
HCl	:	Hydrochloric acid
K_2HPO_4	:	Dipotassium hydrogen phosphate
KH_2PO_4	:	Potassium dihydrogen phosphate
kHz	:	kiloHertz
kPa	:	kiloPascal
kV	:	kiloVolt
L	:	Liter
M	:	Molar
mcl	:	medium chain length
mg mL^{-1}	:	milligram per milliLiter
$MgSO_4$	:	Magnesium sulfate
mL	:	milliliter
ml min^{-1}	:	milliliter per minute

mm	:	milimetre
$MnCl_2.4H_2O$	:	Manganese (II) chloride tetrahydrate
$mol.min^{-1}.cm^{-2}$	:	mole per minute per centimeter square
N	:	Normality
NaOH	:	Sodium hydroxide
nm	:	nanometer
PEGMA	:	Polyethylene glycol monomethacrylate
PHA	:	Poly (3-hydroxyalkanoates)
PMC	:	Poly(malic acid-citric acid)
POME	:	Palm oil mill effluent
PTFE	:	Polytetrafluoroethylene
PV	:	perovskite
PVDF	:	Poly(vinylidene fluoride)
RO	:	reverse osmosis
rpm	:	revolutions per minute
rRNA	:	Ribosomal ribonucleic acid
S80	:	Span 80
SPEM	:	Selective proton exchange membrane
$SrCeO_3$	:	Strontium cerate
$SrTiO_3$	:	Strontium titanate
T80	:	Tween 80
TMS	:	Tetramethylsilane
v/v	:	volume per volume
w/v	:	weight per volume
$ZnSO_4.7H_2O$	:	Zinc sulphate heptahydrate

LIST OF APPENDICES

CHAPTER 1: INTRODUCTION

1.1 Introduction

A surge in the need for clean water worldwide has been more prevalent in recent years due to an increase in water pollution as well as wastewater discharge, prompting research to seek out more efficient and eco-friendly alternatives for water purification. Biopolymers are an attractive substitute because of their low cost, and biodegradable characteristics. PHA or also known as poly (3-hydroxyalkanoates) is a widely studied biological polymer. Microorganisms specifically from the bacteria species produce it intercellularly in an unbalanced growth environment whereby the carbon source is abundant while other nutrients such as nitrogen are deficient. Three major side chains of PHAs are short-, medium-, and long chain lengths depending on the integer of the carbon atoms of respective monomeric unit. In this project, the focus will be on the mcl-PHA because of its high molecular weight and thermo-elastomeric properties. Mcl-PHA is to be used as a polymer matrix to form a selective proton exchange membrane (SPEM). Since pristine mcl-PHA does not conduct protons efficiently, perovskite oxide ($SrTiO_3$) and surfactant (Tween 80) will be used as additives in the membrane matrix to enable the unidirectional flux of protons in the selective proton membrane.

Perovskite-type oxides are known to have a stable structure because of their balanced geometrical arrangement of basic atoms as well as valences. Surfactant on the other hand has a unique structure that comprises of a hydrophilic head and hydrophobic tail. The application of mcl-PHA as a blending matrix for perovskite and surfactant to form a polymer nanocomposite and applied as a selective proton exchange membrane has never been investigated.

Therefore, blending composition of synthesized mcl-PHA, perovskite ($SrTiO_3$) and surfactant (Tween 80) will be investigated in this research.

1.2 Problem Statement

Clean water supply has become a debatable issue globally due to the upsurge in industrial wastewater generation as well as water pollution. Polyhydroxyalkanoates (PHA) have gained widespread interest due to their unique biocompatibility, biodegradability and varied structural composition with physico-mechanical properties closely similar to polyvinyl chloride (PVC) and polyethylene terephthalate (PET). The unique properties of PHA could be beneficial when applied as an integral membrane component in water purification process with practical cost, and devoid of additional harm to the environment; at the same time non-toxic production footprint and promote carbon-neutral usage.

1.3 Hypotheses

(i) Blending of perovskite nanocomposites and surfactant in the mcl-PHA matrix will enhance the proton movement through the polymer matrix.

(ii) The PHA/perovskite/surfactant ratio will determine the rate of proton movement in the selective proton exchange membrane.

1.4 Objectives

(i) To fabricate a selective proton exchange membrane using PHA/perovskite/surfactant nanocomposite film;

(ii) To study the proton conductivity of PHA/perovskite/surfactant nanocomposite film based on the ratio of PHA-to-Perovskite-to-Surfactant and;

(iii) To elucidate the mechanism of proton conductivity in the PHA/perovskite/surfactant nanocomposite membrane.

CHAPTER 2: LITERATURE REVIEW

2.1 Polyhydroxyalkanoates (PHA)

Beijerinck initially described the presence of PHA in bacterial cells in 1888. However, researchers frequently examined PHAs as "lipids" until Lemoigne in 1925 determined that the unspecified material composed by *Bacillus megaterium* was a homopolyester of hydroxyacid, poly-3-hydroxybutyrate (Chodak, 2008). De Smet *et al.* (1983) pioneered the capability of generating different types of PHA relative to the substrate used when cultivating *Pseudomonas oleovorans* in *n*-octane. Growing interest in the advancement of PHAs since the 1970s has been shown in the huge number of studies devoted to understanding and analysing various aspects of this biopolymer.

The biosynthetic pathways to produce PHA by microorganisms are intracellular, triggered by an unbalanced growth environment whereby the carbon source is set to be in excess and essential nutrients like nitrogen, phosphorus, oxygen and magnesium are limited (Annuar *et al.*, 2007; Ishak *et al.*, 2016). The main carbon backbone of PHAs is a monomer hydroxyl group bonded to the carboxyl group of another monomer through an ester linkage (Francis, 2011). There are two categories of PHAs that can be distinguished based on the length of the side chain present: which is short chain length (scl-) and medium chain length (mcl-). Scl-PHA films are known to be rigid, opaque, and brittle in comparison to mcl-PHA films, which tend to be more flexible and translucent (Hacket *et al.*, 2000; VanderHart *et al.*, 2001).

2.2 Mcl-PHA

The Mcl-PHAs are known to comprise 6-14 carbon-atom monomer units. The polyester is produced by the *r*RNA group I *Pseudomonas* species (Lageveen *et al.*, 1988). *Pseudomonas* species can be fed using different fatty acids such as stearic acid, oleic acid and lauric acid which act as precursor substrates to yield structures related to the constituents of the mcl-PHAs (Francis, 2011). The bacteria accumulate intracellular PHA under limited cell growth conditions with abundant carbon sources (Gumel *et al.*, 2012). The Mcl-PHAs that are synthesized by *Pseudomonas* species are usually heteropolymers, where the main monomer is 3-hydroxyoctanoate if grown in a medium consisting of an even number of carbon atoms, and for substrates with an odd number of carbon atoms, 3-hydroxynonanoate is typically formed (Kim *et al*., 2007). There are approximately more than 150 units of mcl-PHA monomers that have been obtained from various *Pseudomonas* species cultured on different carbon sources (Francis, 2011).

The attractive properties of mcl-PHA such as lower crystallinity, a low melting point and high elasticity have enabled this polymer to be promoted as an alternative in different industrial applications. The building blocks of mcl-PHA possess functionalities that allow post-synthetic chemical modification for fine-tuning of properties comprised by the material (Bear *et al*.,1997). They can be depolymerized to chiral monomers for potential usage during the synthesis of antibiotics, vitamins, and other bioactive compounds (Jiang *et al.*, 2006). Rai *et al.* (2011) also reported that mcl-PHAs could be utilised to manufacture adhesives, plasticizers, fibre, medical devices, and bio-carrier for fertiliser release.

2.3 Surfactant

Surfactants are generally known as chemicals that are active either at the surface or at interfaces between two physical phases or in short “surface-active agent” (Moradi & Yamini, 2012). The molecule of a surfactant comprises of hydrophilic and hydrophobic parts, thus known as amphiphilic molecules, which enables them to interact with water and oil phases at the interface. They have a high tendency to migrate to interfaces or surfaces, then orientating their structure to ensure the polar group is in water and the non-polar group is placed away from the water (Moradi & Yamini, 2012).

This chemical compound is essential for reducing the surface tension between two substances, which exist as liquid and solid or liquid and liquid. Surface tension can be classified as a force that causes the liquid surface to act like an elastic membrane that is stretched. Decreasing the surface tension by using surfactants allows the spreading of a liquid over a surface or penetration through porous materials to become easier (Kume *et al*., 2007). Various industries and applications often use surfactants because of their unique set of properties.

In addition, surfactants tend to show other properties compared to only lowering the surface tension; hence they are labelled based on their main usage, like detergent, emulsifier, corrosion inhibitor, etc. (Moradi & Yamini, 2012). Different applications require different properties of the surfactant, hence the characteristics like solubility of water or oil, capability to reduce surface tension, critical micelle concentration (CMC), detergency power, wetting control as well as capacity of foaming could vary significantly; thus, a given surfactant could either perform effectively in certain applications or less effective in others (Myers, 2020).

2.4 Perovskite

A material that has a similar crystal structure to the mineral calcium titanium oxide ($CaTiO_3$) is known as perovskite. A perovskite compound has the general chemical formula ABX_3, where A and B are cations and X is an anion that bonds to them directly. The most common type of perovskite is the oxide type, which has a general formula of ABO_3. There are certain cationic characteristics that are required to form a stable perovskite oxide. A-type cations are 12-coordinated by oxygen with a large ionic radius, similar to the oxygen ion, whereas B-type cations are 6-coordinated by oxygen while having a small ionic radius and are situated in the octahedral holes between the closed-pack AO-layers (Hooshyari *et al.*, 2020). A and B-types are usually rare alkaline earth metals and first-row transition metals (Grabowska, 2016).

In a perovskite, the atoms are specially oriented, hence high stability can be obtained. Research literature has emerged recently detailing the high proton conductivity of perovskite-type oxide in wet atmospheres at high temperatures. Furthermore, due to the vast range of ferro-, piezo-, and pyroelectrical properties and electro-optical effects shown in perovskite oxides, they have been incorporated as electronic, structural, magnetic, and refractory materials in many technological applications (Grabowska, 2016). Some examples of perovskite oxides are $BaCeO_3$, $BaZrO_3$, $SrCeO_3$ and $SrTiO_3$ (Voorhoeve *et al.*, 1997).

2.5 Water Purification

A global increase in water pollutants has caused a significant increase in death and diseases within the human population whereby nearly 14000 people have died daily due to this pollution, and almost 80 % of the global population has begun facing problems relative to the clean water supply chain and security (Vorosmarty *et al*., 2010). Emerging water purification techniques are one of the solutions to the water pollution problem. In recent years, there is a significant increase in the types of water purification processes (Bolisetty *et al.*, 2019). Among them, the commonly used ones are reverse osmosis (RO), adsorption, sedimentation, and membrane filtration.

The classic system of reverse osmosis (RO) comprises of four steps which are pretreatment, pressurization, salt parting and post-treatment (Shenvi *et al.*, 2015). Initially water is pretreated by using different chemicals prior to pressurization and then separated for further purification which finally undergoes post treatment to decontaminate any other impurities (Ahmad & Azam, 2019). Adsorption is a surface phenomenon where the water interacts with the surface of the solid adsorbent *via* chemical or physical bonding to remove contaminants. Activated carbon usually is used as the adsorbent in this case due to its characteristics i.e., big porous surface area with a controllable pore structure, low acid, or base reactivity and also thermostability which enables high removal efficiency of contaminants (Foo & Hameed, 2009).

Sedimentation technique is designed to gather solid contaminants, slurries produced by rainwater and snowmelt, sludge and wastewater that flows gravitationally through the sewers. The hydraulic load of the system ensures a high efficiency of separation to ensure semi-purified water is produced (Ochowiak *et al*., 2017). Based on Davidson & Summerfelt (2005), a minute change in the design of the separator could provide a significant improvement in the water purification system. Another approach, usually applied in tandem, would be utilizing the membrane filtration system in the subsequent step of water purification. Contaminants in the water fed into the membrane system would accumulate as retentate, which is then eliminated. All these methods, either applied singly or in combination, provide wide opportunities for clean water to be obtained.

2.6 Membrane Filtration

At present, separation technologies are widely used, especially membrane filtration in water treatment as well as to treat wastewater. Technology using the membrane has grown into the area of secondary or tertiary treatment for municipal wastewater and even oil field-related water. In the membrane filtration process, the membrane plays the role of a barrier, whereby it separates two phases and restricts the transport of different chemicals *via* selectivity. Specified characteristics can also be introduced when producing the membrane such as carrying either a positive, negative, or neutral charge. Transport through the membrane is often affected by convection or diffusion of each molecule as well as induction by the gradient difference, either chemically or electrically (Chen *et al*., 2006).

Established membrane filtration processes in the industry are microfiltration, nanofiltration, ultrafiltration and reverse osmosis (RO). However, these treatment techniques are known to be highly dependent on environmental factors like temperature, feed composition and level of oxygen. Moreover, an intensive amount of energy is consumed in the course of these treatment processes. A substantial quantity of greenhouse gas emissions is also produced during (bio)chemical conversion of organics or nutrients in the waste effluent e.g., carbon dioxide (CO_2) (Hube *et al*., 2020). To help reduce the generation of wastewater and toxic byproducts during the upstream processes, ion-exchange membrane filtration is beginning to be used largely in an array of industrial applications such as water desalination through the usage of conventional electrodialysis and eliminating of toxic compounds from wastewater generated by the industry (Strathmann, 2010).

2.7 Selective Proton Exchange Membrane (SPEM)

Ion exchange membranes can be classified into two distinct types; cation-exchange membranes that comprises of negatively charged groups fixed to the matrix of the polymer, and anion-exchange membranes which contain positively charged groups fixed within the polymer matrix (Strathmann, 2010). Selective Proton Exchange Membrane (SPEM) is classified as a semipermeable membrane that aids the transport of protons across (Walkowiak-Kulikowska *et al*., 2017). It can be categorized as a cation-exchange membrane, whereby the negative charges present are electrical equilibrium with the mobile cations inside the interstices of the polymer. Moving anions are not able to enter the polymer matrix due to the similarity in charge with the fixed ions. As a result of the exclusion of moving anions, the cation exchange membrane only allows the specific cations passing through the membrane (Strathmann, 2010).

Recently, membrane matrices that are mixed with nanoparticle additives have emerged. They are also known as polymer-nanocomposite membranes. These mixed matrix membranes pose a great advantage to industry because the cost is low as well as the ease of fabricating the composite. The inorganic material present within the membrane enables better mechanical strength and functional properties, hence enabling the membrane to be used in water treatment due to its high selectivity, targeted functionalities, and enhanced thermal and chemical stability (Pendergast & Hoek, 2011).

The nanoscale characteristic of the additive in the polymer matrix increases the surface area and activity within the membrane, hence making it an effective substitute for the common activated carbon used in water and wastewater treatment. Yan *et al*., (2005) developed ultrafiltration mixed matrix membranes using alumina nanoparticles with approximate size 10 nm added to a casting solution during phase inversion of poly(vinylidene fluoride) (PVDF). The density and size of the pores were not altered; however, an increment was observed for the following characteristics: hydrophilicity, permeability of water, resistance to fouling, flux recovery and mechanical stability. Polyaniline nanofibers had been added to commercial ultrafiltration membranes ranging from 1-15 weight%, and an increase was observed for the water permeability, selectivity, and surface wettability of the membranes (Fan *et al*., 2008).

2.8 Biopolymer based film composite as SPEM

Recently, researchers have begun to develop membranes using naturally sourced materials. This is due to the high cost of production and increment in secondary pollution within the environment (Winfield *et al.*, 2013). Chitosan, cellulose and mcl-PHA are some of the known biopolymer alternatives that have been studied. The deacylated derivative of chitin is known as chitosan (CT), which can be found commonly in the exoskeleton of insects, shells of sea creatures and even cell walls of fungi. Prominent characteristics such as hydrophilicity, biocompatibility, non-toxic, stable thermally and chemically enabled CT to be used as a SPEM (Rao *et al.*,2007; Dash *et al.*, 2011; Suginta *et al.*, 2015). To further increase conductivity in CT modification *via* blending, sulphonation and cross-linking can be carried out. The presence of free amino and hydroxyl groups within the chitosan structure simplifies the modification process.

Harewood *et al.* (2017) reported that to improve proton conductivity as well as reduce swelling of CT, the cationic biopolymer was blended and cross-linked ionically with an anionic copolymer poly (malic acid-citric acid) (PMC). Increased proton conductivity could be observed. Cellulose on the other hand is another good option to be used for SPEM production. It has high mechanical strength, able to retain water efficiently and stable thermal properties. Grafting and crosslinking are the two common techniques used to modify cellulose into a good proton conductive membrane. The three hydroxyl groups present in every anhydrous-glucose unit also contribute to aiding the movement of proton (Samaniego & Espiritu, 2022).

Based on a study conducted by Choi *et al.* (2003), a cellulose based membrane which was synthesized by using *Acetobacter* sp strain JH232 was grafted with acrylic acid (AAc) *via* UV-irradiation. Scanning electron micrographs showed that AAc filled the porous structure of cellulose hence structural density was increased. The mechanical strength of the membrane was improved as well due to the cross-linking process. Increase in ion exchange capacity was observed, owing to AAc possessing an anionic head group.

The Mcl-PHA is known for its resistance to rapid hydrolytic degradation. However, it is nonconductive in its pristine state. Compositing mcl-PHA with a highly conductive material could increase its electro-conductive properties (Hindatu *et al*., 2017). Inorganic materials are among the frequently suggested materials used to improve the mechanical and proton conductivity of the membrane (Hooshyari *et al.,* 2020).

Perovskite-type oxides with ABO_3 structure are one of the inorganic materials used as an additive in selective proton membranes because of their efficient proton conductivity, as well as notable mechanical and thermal stability (Selvakumar *et al*., 2019). A few examples of mcl-PHA modification include its use as a support membrane for carbon nanotubes (CNT) to enhance ion movement (Hindatu *et al*., 2017), grafting PEGMA onto mcl-PHA for electrode modification (Yusuf *et al*., 2019) and graphene grafted on mcl-PHA for the use of different biomaterials such as biosensors and nerve repair conduits (Yao *et al*., 2018). All modified mcl-PHAs showed a significant increase in proton conductivity compared to the neat PHA form (Hindatu *et al*., 2017; Yusuf *et al*., 2019; Yao *et al*., 2018).

CHAPTER 3: MATERIALS AND METHODS

3.1 Materials

3.1.1. Microorganisms

Pseudomonas putida BET001, isolated from palm oil mill effluent (POME) (Gumel *et al*., 2012), was utilized as the producer in the biosynthesis of medium-chain-length polyhydroxyalkanoates (mcl-PHA). The microorganism was acquired from the Bioprocess and Enzyme Technology Laboratory, Institute of Biological Sciences, Faculty of Science, University of Malaya.

3.1.2. Carbon source

Lauric acid with a carbon chain length of 12 (C12) was used as the main carbon source to produce mcl-PHA in the E2 medium.

3.1.3. Media

A two-stage culture system was used in the process of mcl-PHA production which includes two production media i.e., rich medium (Table 3.1) and E2 medium (Table 3.2). The following compounds are the ingredients for each media formulation:

Table 3.1:Rich Medium

Compounds	Mass dissolved 1 L in distilled water (g)
Nutrient broth (MERCK)	8.0
Yeast extract	10.0
Ammonium sulphate	5.0

Table 3.2: E2 Medium (Lageveen *et al*., 1988)

Compounds	**Mass dissolved in 1 L distilled water (g)**
Ammonium sodium phosphate dibasic tetrahydrate (**A**)	3.5
Lauric acid	10.0
K_2HPO_4	5.73
KH_2PO_4	3.7
Mineral Solutions	**Volume in 1 L distilled water (ml)**
0.1 M $MgSO_4$	10.0
Trace elements (Refer to **(B)**)	1.0

(A) The formulation for PHA accumulation phase requires 3.5 g L^{-1} (0.35 % w/v) of ammonium sodium phosphate dibasic tetrahydrate as the limiting nitrogen source in the medium of E2.

(B) The composition of elements present in the trace elements solution is shown in Table 3.3:

Table 3.3: Element composition in trace elements solution (Lageveen *et al*., 1998)

Elements	Mass dissolved in 500 mL of 1 N HCl (g)
$FeSO_4.7H_2O$	1.39
$MnCl_2.4H_2O$	0.99
$CoSO_4.7H_2O$	1.41
$CaCl_2.2H_2O$	0.74
$CuCl_2.2H_2O$	0.08
$ZnSO_4.7H_2O$	0.14

3.1.4. Setup for Incubator and Shaker

Cultivation of bacterial cultures was carried out in shake flasks using Hotech model 721 orbital shakers (Hotech Instruments Corp., Taiwan). Cell growth and PHA-accumulation phase of the cultures were conducted in an incubated environment at 35 °C ± 0.2. Flasks were shaken at 200 rpm.

3.1.5. Sterilizer

Autoclave brand Tomy SS-325 (Japan) was used in the steps that required sterilization. Temperature and pressure settings were specifically set to 121 °C and 103 kPa, respectively, for a duration of 15 minutes.

3.1.6. Centrifugation

Centrifugation of liquid volume 50 ml was performed by using Thermo Scientific Sorval RC-5C ultracentrifuge (U.S.A).

3.1.7. Ultrasonicator (Water Bath)

Dispersion of different concentrations of perovskite and surfactant in PHA polymer solution was conducted by using an ultrasonicator (Elmasonic P 30 H, Germany).

3.1.8. Rotary Evaporator (RotaVap)

Polymer solution was concentrated using BUCHI R-210 rotavapor (Switzerland).

3.1.9. Analytical Instruments

i. Gas Chromatography-Mass Spectrometer (GCMS)

PHA quantification and monomeric composition determination were carried out using the Shimadzu GCMS-QP 2010 Plus, fitted with a 5 % phenyl-based column (30 m x 0.25 mm ID) (ZEBRON. ZB5) and mass spectrometer detector. Helium gas was used as the mobile phase at a flow rate of 2.734 ml min^{-1}. Temperature set for both injector and detector were at 200 °C and 280 °C, respectively. Oven ramping was set from 50 to 280 °C at 10 °C min^{-1}.

ii. ^{1}H-Nuclear Magnetic Resonance (^{1}H-NMR)

^{1}H-NMR, JEOL JNM-LA 400 FTNMR spectrometer at 400 MHz, was used to elucidate the PHA chemical structure in ambient temperature (25 °C). 2.0 mg mL^{-1} of PHA-$CDCL_3$ was used in the measurement, containing tetramethylsilane (TMS) as an internal reference.

iii. Fourier Transform Infrared Spectroscopy (FTIR)

Perkin Elmer FTIR-Spectrum 400 was used to perform the FTIR analysis for neat-PHA and PHA-PV-TW samples to determine the presence of functional groups. Sample films of each sample were placed on the monolithic diamond ATR probe and fastened against the diamond crystal plate using a force adapter.-The spectra were recorded from 4000 to 550 cm^{-1} with a 4 cm^{-1} resolution and 8 scans at ambient temperature.

iv. Thermogravimetric Analysis (TGA)

Analysis of thermal properties such as initial thermal degradation (T_d) and thermo-degradation kinetic of neat-PHA and PHA-PV-TW samples were conducted by Thermogravimetric Analysis 4000 (TGA4000) (Perkin Elmer). Approximately, 20 mg of sample was heated from 30 to 500 °C at 10 °C min^{-1}.

v. Differential Scanning Calorimetry (DSC)

Differential scanning calorimetry (DSC 8825/700) (Mettler Toledo) analysis was carried out to identify the glass transition temperature (T_g) and melting temperature (T_m) of all samples. Temperature range conducted for the analysis was between -60 to 80 °C with a heating rate of 10 °C min^{-1}.

vi. Field Emission Scanning Electron Microscopy (FESEM)

Surface of neat-PHA and PHA-PV-TW samples were examined in detail by using the field emission scanning electron microscopy (FESEM) (SU8220) (Hitachi). Observation was performed under vacuum conditions at an acceleration rate of 2 kV. Different magnifications ranging from 250 x to 5.00 were observed.

vii. pH Meter

Measurements of pH value change to analyse proton transfer across the membrane were conducted using the microprocessor-based pH bench meter (HI 2211) (HANNA Instruments).

3.1.10. Analytical Reagents

i. Acidified methanol

For PHA methanolysis the following solution was made; 85 ml of cold methanol was mixed with 15 ml of concentrated sulfuric acid and stored in the chiller at 4 °C.

ii. Surfactant

Tween 80 (Sigma-Aldrich, U.S.A., CAS-9005-65-6) or also known as Polysorbate 80 was used in the process of dispersion to produce an evenly distributed membrane. Span 80 (Sigma-Aldrich, U.S.A., CAS-1338-43-8) was also used in the membrane preparation for comparison study of proton transport.

iii. Perovskite

Strontium titanate ($SrTiO_3$) (Sigma-Aldrich, U.S.A., CAS-12060-59-2) nano powder with a particle size < 100 nm and purity of ≥ 99% was incorporated into the PHA membrane.

iv. Dichloromethane (DCM)

Dichloromethane, ACS Reagent (Merck, CAS-320269) with ≥ 99.9 % purity, was used as solvent to dissolve and mix PHA solution with perovskite as well as surfactant.

3.2 Methods

3.2.1. Stock culture preservation

Bacteria strain was kept at a -20 °C temperature in an Eppendorf tube containing glycerol solution (Table 3.4). Stock preparation was carried out by combining 0.5 ml of rich medium and freshly cultured *P. putida* with 1.5 ml of glycerol in the Eppendorf tube. To ensure constant availability of the strain while the study was carried out, multiple stock preparations were made (Ishak *et al*., 2022; Sirajudeen *et al*., 2021; Gumel *et al*., 2014).

Table 3.4: Glycerol solution for culture preservation

Component	Percentage (*v/v*)
Glycerol (100 %)	65.0
$MgSO_4.7H_2O$	10.0
Tris base (1 M)	2.5
Distilled water	22.5

3.2.2. Preparation of culture media for mcl-PHA production

Based on Table 3.1, all listed compounds were combined and dissolved in distilled water to form the rich medium. Then, before rich medium underwent steam sterilization, additional sterile distilled water was added to it until the pre-determined volume (Ishak *et al*., 2022; Sirajudeen *et al*., 2021; Gumel *et al*., 2014).

The E2 medium on the other hand was prepared through a combination of two solutions *viz*. the phosphate buffer and fatty acid blend. A phosphate buffer was initially prepared using two kinds of phosphate salts, which were then dissolved in distilled water. Adjustment of pH to 7.0 ± 0.03 was conducted prior to placing the buffer into the autoclave for steam sterilization. Next, preparation of fatty acid solution was carried out by firstly dissolving it in sterilized low concentration NaOH solution. It was to ensure evaporation of short-chain fatty acids due to high temperature conditions were reduced (Ishak et al., 2022; Sirajudeen et al., 2021; Gumel et al., 2014).

Then, H_2SO_4 solution was used to neutralize excess NaOH in the fatty acid solution, and to adjust the pH to 7.0 ± 0.03. Both solutions were combined aseptically at room temperature, alongside ammonium salt, trace elements and $MgSO_4$ solutions that were sterilized separately to the final concentration and volume of the E2 medium prior to bacterial inoculation. The precaution was taken to prevent precipitation among the E2 medium components due to high temperature and pressure conditions during steam sterilization process (Ishak *et al*., 2022; Sirajudeen *et al*., 2021; Gumel *et al*., 2014).

3.2.3. Biosynthesis of mcl-PHA

Pseudomonas putida BET001 was cultured using batch fermentation technique to produce mcl-PHA with lauric acid as the main carbon and energy source. The culture system was divided into two stages i.e., cell growth stage and PHA accumulation phase. Cultivation setup and media preparation were described in sections 3.1.4 and 3.2.2, respectively. Summary of method conducted is as follows:

Cell growth phase began when bacterial culture was grown in the rich medium for 24 hours. After that, biomass cells were harvested under aseptic condition *via* centrifugation at 4 °C, washed with saline solution (0.9 % *w/v*) then aseptically transferred to the E2 medium to undergo PHA accumulation phase. 1.0 % (*w/v*) of fatty acid and 0.35 % (*w/v*) ammonium sodium phosphate dibasic was added into the medium as a carbon and nitrogen source, respectively. Cultivation lasted for 24 hours at ambient temperature, before being harvested once again by centrifugation at 4 °C (Ishak *et al*., 2022; Sirajudeen *et al*., 2021; Gumel *et al*., 2014).

3.2.4. Biomass collection and removing excess fatty acids

After E2 medium was incubated for 24 hours, harvesting of cells were conducted by centrifugation at 8000 ×*g* (Thermo Scientific Sorvall RC-5C Plus ultracentrifuge) at 4 °C. Rinsing of pellets were carried out twice using 0.9 % (*w/v*) saline solution. Then, the washed biomass pellet was placed in the oven to dry at 50 °C until constant weight. Fatty acid residue was discarded by washing the biomass in *n*-heptane (Ishak *et al*., 2022; Sirajudeen *et al*., 2021; Gumel *et al*., 2014).

3.2.5. Solvent extraction and purification of PHA

Extraction process of PHA was carried out by refluxing 1.0 g dried cells in acetone (100 ml) for 4 hours at 25 °C ± 2.0. Mixture was then filtered using Whatman filter paper No.1. After filtration, the pellets were recollected and underwent two additional cycles of solvent reflux in 50 ml acetone for another 4 hours. Repetitive cycles were conducted to ensure maximum PHA extraction from the biomass. Each filtered solution from all three-cycle was combined, and then concentrated by utilizing the rotary evaporator until approximately 10 ml remained (Ishak *et al*., 2022; Sirajudeen *et al*., 2021; Gumel *et al*., 2014).

After that, the concentrated solution containing the polymer was mixed with cold methanol (1:7) to induce PHA precipitation, and the mixture was allowed to stand for 30 minutes. Precipitated PHA was centrifuged at 1920 ×*g* for 10 minutes to recover suspended fraction. Solvent mixture was poured out and precipitated PHA remained at the bottom. By re-dissolving the recovered PHA with small volume of acetone followed by re-precipitation in excess methanol, high purity PHA can be obtained. The previous step can be carried out multiple times to achieve a highly purified PHA. The polymer solution was cast onto a glass petri dish and left to air-dried until constant weight (Ishak *et al*., 2022; Sirajudeen *et al*., 2021; Gumel *et al*., 2014).

3.2.6. Methanolysis of PHA for GCMS analysis

0.05 g PHA was dissolved in 3 ml filtered dichloromethane in a tube that was screw capped and sealed with PTFE tape to prevent solvent evaporation during heating. Then, 3 ml of acidified methanol with a 15 % (*v/v*) sulfuric acid content was transferred into the polymer solution. The temperature within the heating block (Wistherm HB-48) was set at 100 °C for 140-minute. The tube was shaken occasionally for homogeneity. Upon completion of heating, the tube was left to cool at room temperature, and followed by the addition of 3.0 ml distilled water. The mixture was vortex-mixed and allowed let to separate into two immiscible layers. Subsequently, the bottom layer of the mixture *viz.* the organic phase was recovered and placed into a small vial containing sodium sulphate anhydrous. The small amount of sodium sulphate anhydrous aids in removing any traces of moisture trapped in the organic phase. Finally, the organic phase composition was analysed using gas chromatography mass spectrometer (GCMS) (Ishak *et al*., 2022; Sirajudeen *et al*., 2021; Gumel *et al*., 2014).

3.2.7. Fabrication of selective proton exchange membrane

The membrane fabrication technique was developed entirely from nil through the initial phase of trial-and-error. Pre-determined mass percentages $SrTiO_3$ (designated as PV) and Tween 80 (designated as T80) ranging from 0.01 - 0.0025 % (*w/v*) and 1.5 – 4.5 % (*w/v*) respectively, were dispersed with PHA (0.4 g) in dichloromethane (DCM) using ultrasound-assisted technique in water bath sonication (Elmasonic P sonicator). Setup for ultrasonication was at 30 °C, 37 kHz, 80 % power for 40 minutes.

Water inside the bath was changed when necessary to ensure temperature remained constant throughout the sonication period. After ultrasonication, the solution was vortexed to obtain a homogenous mixture prior to casting on a petri dish (3.6 cm diameter), and to be air-dried to a constant weight. All steps above were repeated when fabricating membranes using Span 80. Neat-PHA film was prepared using a similar technique to the PHA blends. The thickness of the membrane was measured using a digital micrometer (Mitutoyo, ±0.001 mm) based on the average of three random measurement points. All membranes showed a thickness of approximately 0.32 ± 0.05 mm.

3.2.8. Measurement of proton flux across membrane

A double-chambered vessel comprising two H-shaped glass bottles, with the height and diameter 6.5 cm and 4.5 cm, respectively, was utilized as the setup for the proton movement analysis. Between both chambers, each membrane (3.6 cm diameter) was placed for every experimental analysis. Initially, left and right chambers were filled with 60 ml ultrapure water and left to equilibrate for 15 minutes while being stirred at a constant rate of 100 rpm. Then, 0.6 ml of concentrated HCl (0.1 M) was added to the left chamber. pH changes in the right chamber were recorded every 30 seconds until it reaches a plateau. The same experimental setup and procedure was applied for proton flux analysis in tap water. The experiment was conducted at 25 ± 0.1°C. The photograph of the double-chamber vessel setup is shown in Appendix *A*.

CHAPTER 4: RESULTS AND DISCUSSION

4.1 Mcl-PHA structure

4.1.1. Gas Chromatography Mass Spectrometry (GCMS)

The monomeric composition analysis of neat PHA was conducted–by using gas chromatography mass spectrometry (GCMS). The methylated 3-hydroxyalkanoates mixture in the sample is separated into individual fractions by controlling the heating rate and nitrogen flow rate of the column chromatography. As stated in the previous section 2.2, mcl-PHA may consist of monomers ranging from C_6 – C_{14}. Figure 4.5 shows the three retention times detected in the analyzed sample indicating three major monomers of mcl-PHA. Retention time (a) 12.783 min is assigned to methyl 3-hydroxyoctanoate (C_8), (b) 15.566 min to methyl 3-hydroxydecanoate (C_{10}) and (c) 18.048 min to methyl 3-hydroxydodecanoate (C_{12}). Methyl 3-hydroxyhexanoate (C_6) and methyl 3-hydroxytetradecanoate (C_{14}) were not detected probably due to their residual amount in the prepared samples.

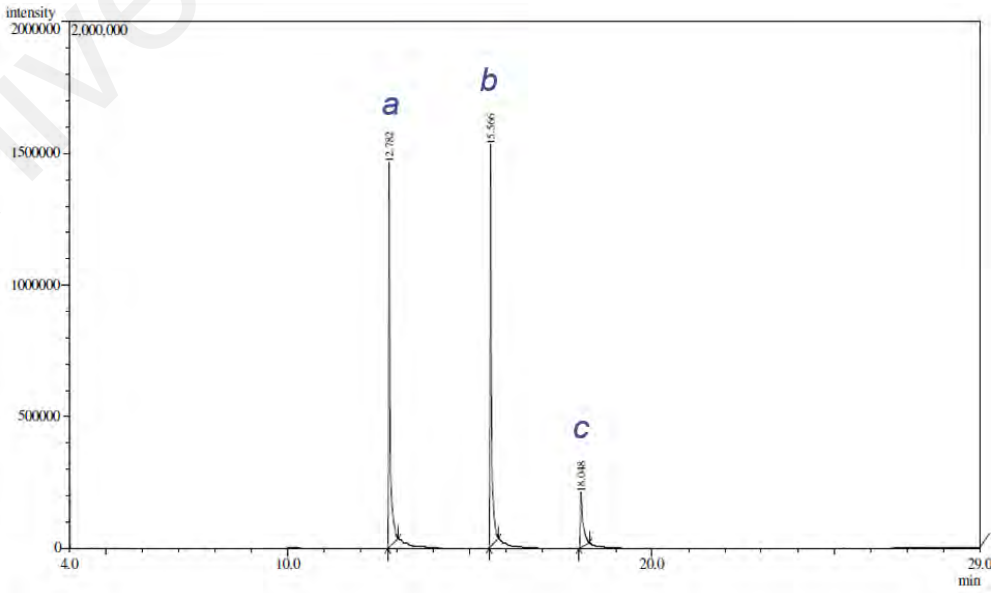

Figure 4.1: Gas chromatogram of mcl-PHA

4.1.2. ^{1}H-NMR

Proton NMR was used to analyse the chemical structure of PHA produced with internal standard tetramethylsilane as reference. The analysis facilitates the identification of the environments surrounding the carbon atoms within mcl-PHA hence allowing the determination of each carbon's position ultimately leading to structural elucidation, which provide benchmark for subsequent corroborative structural and properties studies. Peak ***d*** (δ 2.5 ppm) and ***e*** (δ 5.2 ppm) are both multiplet peaks. These peaks represent the methylene and methine protons located at the α and β carbons, respectively. Duplet peak ***c*** (δ 1.6 ppm) on the other hand, is neighboring to the β carbon (***e***) in the side chain. Peak ***b*** (δ 1.3 ppm) and triplet ***a*** (δ 0.9 ppm) are classified as the methylene protons and terminal methyl proton placed at the end of the side chain (Chung *et al.,* 2011; Gumel *et al.,*2012; Liu *et al.,*2011). Peak signals distinguished were almost identical to mcl-PHA with similar structures reported in previous studies.

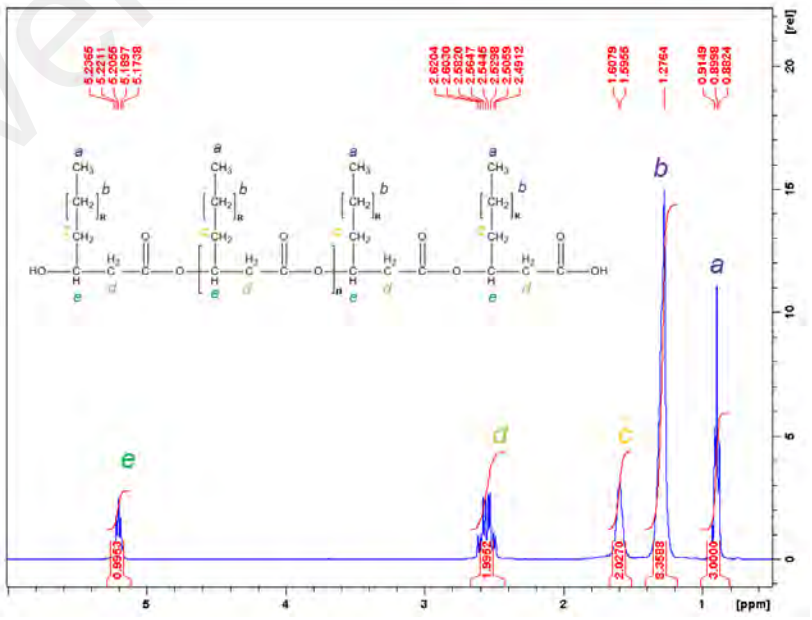

Figure 4.2: ^{1}H-NMR of mcl-PHA produced

4.2 FTIR analysis of PHA-PV-T80 composites

Both neat-mcl PHA (control) and Polyhydroxyalkanoate-Perovskite-Tween 80 (PHA-PV-T80) composites yield signal peak of the representative moiety i.e., intense peak at ≈ 1730 cm^{-1} that signifies the stretching band of carbonyl group (C=O) of PHA and T80 (Guo *et al.,* 2013; Pramod *et al.,* 2015). Two absorption peaks at 2850 and 2925 cm^{-1} are both representing the stretching modes of anti-symmetric and symmetric CH_3 and CH_2 of alkyl chain, respectively. Meanwhile, peak signals from 1000 -1500 cm^{-1} stipulate the occupancy of CH_2, CH_3, -C-O-C and -C-C-. Bands 1050 – 1280 cm^{-1} specify the symmetric and antisymmetric stretching mode of C-O-C in PHA (Guo *et al.,* 2013). The absorption peak located near 720 cm^{-1} is assigned to the CH_2 side chain of PHA.

Increasing intensity of peak 1050 cm^{-1} and the occurrence of big hump around 3700 cm^{-1}, as shown by arrows in Figures 4.3a and 4.3b, indicate stronger presence of T80 in the PHA-PV-T80 composites. The former represents the ester bonds while the latter represents the hydroxyl groups of the T80 hydrophilic head. Metal oxide bands usually appear within the range of 500 – 800 cm^{-1} depending upon the perovskite phase (Raja *et al.*, 2019). Overlapping of peaks occur between the CH_2-side chain and metal oxide in the PHA-PV-T80 composites, hence broader peaks at ≈ 800 cm^{-1} were observed as shown by dashed arrow in Figures 4.3a and 4.3b; attributed to the intercalation of perovskite particles within the PHA matrix promoted by the polarization effects between the former and the latter. A pronounced difference is also evident in Appendix *B*.

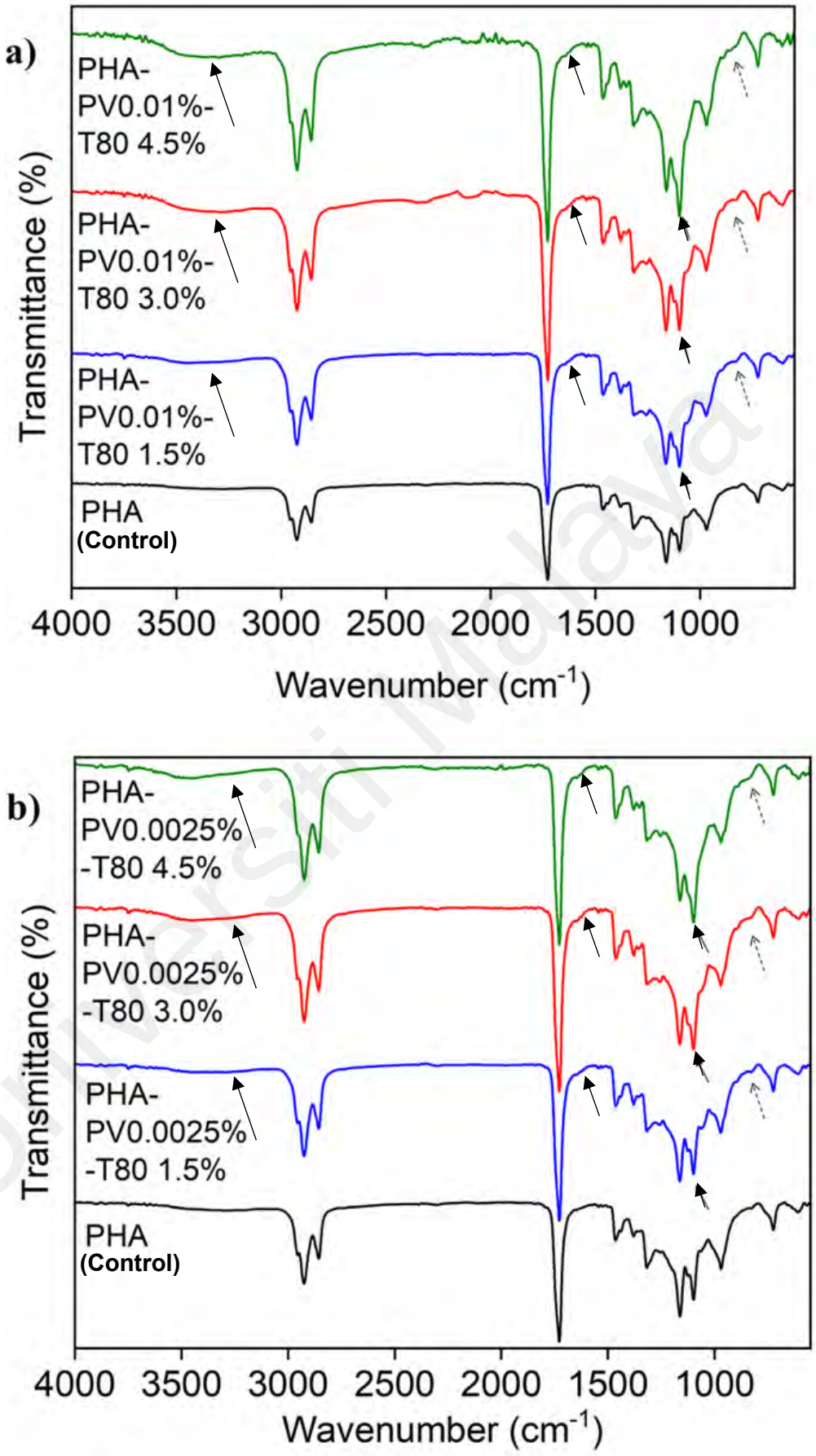

Figure 4.3: FTIR spectra of neat mcl-PHA and (PHA-PV-T80) composites; a) high PV and b) low PV concentration with increasing T80 amount

4.3 XRD analysis of PHA-PV-T80 composites

Neat mcl-PHA and PHA-PV-T80 composites exhibit two diffraction peaks *viz.* 19.5˚ and 21˚, as shown in Figure 4.4. These peaks represent the side-chain crystallization of PHA, which occurs in the rigid regions within the polymer matrices (Ishak *et al.,*2021). On the other hand, perovskite yields 2θ = 22.5˚, 32˚, 40˚, 46.6˚, 57.6˚, 67.7˚and 77.3˚(Appendix *C*). Assignments of these peaks are corroborated by previous studies (Raja *et al.*., 2019; Sirajudeen *et al.*., 2021).

The presence of perovskite within the PHA matrix may induce additional formation of rigid regions in the polymer matrix, thus facilitating side-chain crystallization, evident from the diffraction peaks of PHA-PV0.01%-T80 (Figure 4.4a) composites, which are stronger in intensity as compared to PHA-PV0.0025%-T80 (Figure 4.4b). Higher concentration of perovskite within PHA-PV0.01%-T80 composites promote greater side-chain crystallization.

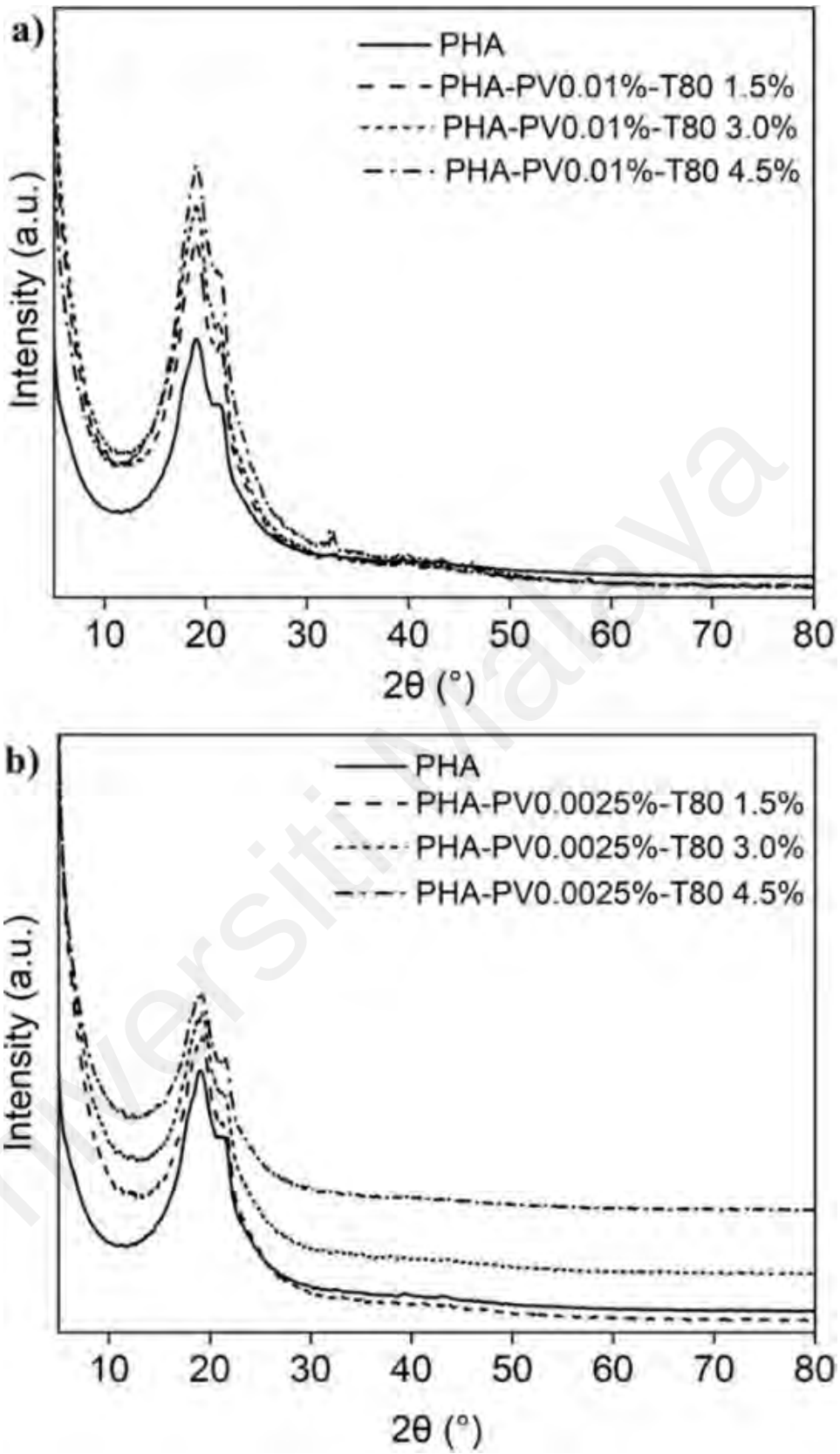

Figure 4.4: X-Ray diffractograms of neat mcl-PHA and PHA-PV-T80 composites; a) high PV concentration and b) low PV concentration with increasing T80 amount

4.4 FESEM analysis of PHA-PV-T80 composites

Homogenous dispersion of perovskite (PV) and Tween 80 (T80) within film matrix can be observed from the FESEM images of PHA-PV-T80 composites in Figure 4.5; indicating the utility of ultrasonication dispersion technique applied in the fabrication process. Observable aggregation of powder or liquid phase is absent in the images. Generally, all composites exhibit non-uniform surface morphology compared to the smooth and uniform neat mcl-PHA owing to broader presence of rigid regions within the composite matrix (Mohamed *et al.,* 2021).

It is worth noting that a more textured morphology was observed in the PHA-PV0.01%-T80 4.5% sample (Figure 4.5e); attributed to the extensive side-chain crystallization concomitantly the increase in rigid regions, as previously discussed. The maximum feasible amounts for incorporation into the composite without unwanted aggregation were determined at 4.5 % for T80 and 0.01 % for PV. These values provided the upper limits for subsequent experimental procedures. FESEM micrographs with higher magnifications are provided in the *Appendices* (Appendix *D-F*).

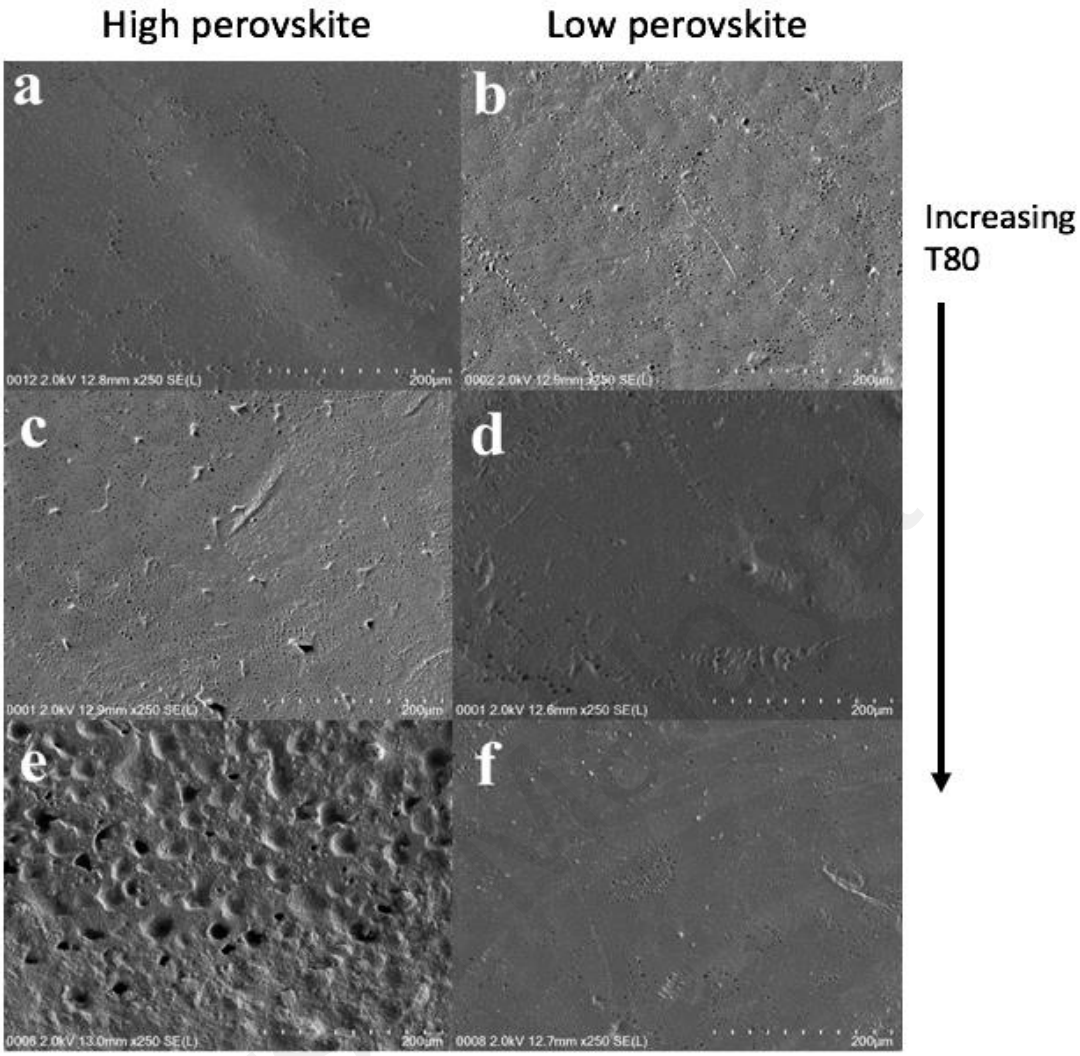

Figure 4.5: FESEM micrographs of PHA-PV-T80 composites; a) PHA-PV0.01%-T80 1.5%, b) PHA-PV0.0025%-T80 1.5%, c) PHA-PV0.01%-T80 3.0%, d) PHA-PV0.0025%-T80 3.0%, e) PHA-PV0.01%-T80 4.5% and f) PHA-PV 0.0025%-T80 4.5%

4.5 Thermal analysis of PHA-PV-T80 composites

Two glass transitions (denoted as T_{g1} and T_{g3}) evident in the DSC thermograms at ≈ -50 and 10 °C (Figure 4.6a and b) were ascribed to the base polymer, i.e., mcl-PHA (Ishak *et al.,* 2022). One additional glass transition (denoted as T_{g2}) at temperature range of -24 to -17 °C was found in the PHA-PV-T80 composites only. It is hypothesized that incorporation of PV in the composites resulted in the increase of rigid regions across the polymer matrix, thus making the composite films sturdier while allowing the PHA as base material to retain some degree of flexibility. The melting temperature (T_m) of PHA-PV-T80 showed slight changes as compared to neat mcl-PHA (Fig. 4.6a and b), which is suggested to arise from the effect of T80 intercalation in-between PHA chains, thus resulted in sooner melting process of the rigid regions. The presence of unsaturated alkyl chains in T80 may lead to a decrease in the PHA side chains interaction crucial for retaining the integrity among its main chains during temperature increase.

Figure 4.7a and b show the results of thermogravimetric analysis for neat mcl-PHA and-PHA-PV-T80 composites. Neat mcl-PHA degrades at a temperature of 250 ℃, which is in agreement to a previous study (Ishak *et al..*, 2015). Meanwhile PHA-PV-T80 composites were observed to have a slightly higher thermal degradation temperature (T_d) from 260 - 275 ℃, indicating that the blending of PHA with surfactant and perovskite improved its thermal stability at higher temperature. The thermal properties of the PHA composite films remained unaffected upon the conclusion of proton flux experiments. This can be proven from insignificant changes observed in the DSC and TGA thermogram (Appendix *G* and *H*).

It implies the absence of irreversible physical/chemical modification or impairments of the composite membranes subsequent to the proton transfer experiment. Overall, based on spectroscopic-, X-ray diffraction, morphological- and thermal studies, it can be concluded that the fabricated composite films exhibit good physical characteristics for potential application as membrane material.

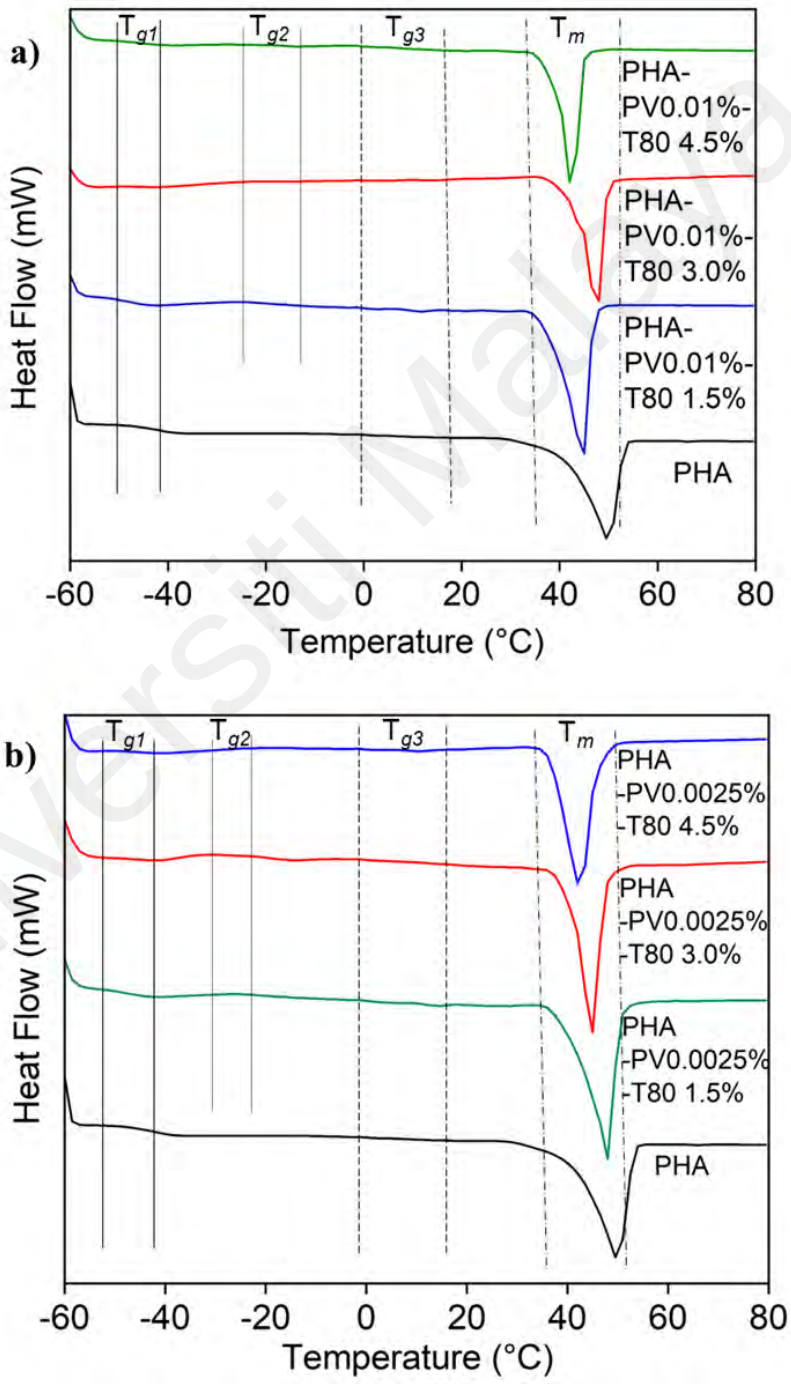

Figure 4.6: DSC thermograms of neat mcl-PHA and PHA-PV-T80 composites; a) high PV and b) low PV concentration with increasing T80 amount

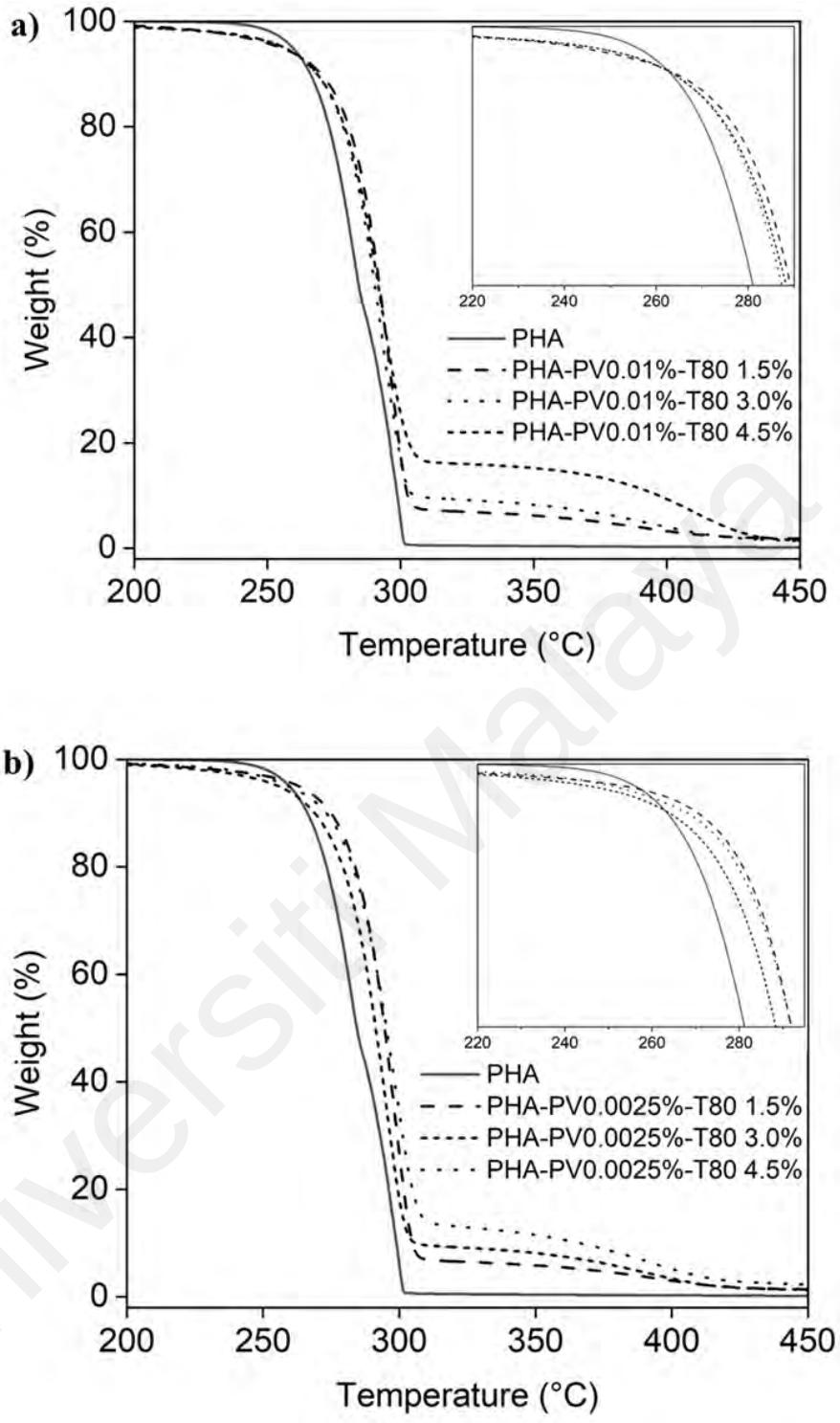

Figure 4.7: Thermal weight loss profile for neat mcl-PHA and PHA-PV-T80 composites; a) high PV concentration and b) low PV concentration with increasing T80 amount

4.6 Proton Flux Analysis

Figure 4.8 shows the comparison of proton transfer in ultrapure water through PHA-PV-T80 composite films, and the proton flux ($\times 10^{-4}$ mol.min^{-1}.cm^{-2}) for each film (Table 4.1). Neat PHA film, Nafion and PHA composites incorporated with Span 80 (S80) was also tested for comparison. It can be seen that composite with T80 can transport protons at a higher efficiency as compared to other tested films, including neat mcl-PHA and Nafion (standard membrane used as control). It is suggested that extensive molecular interaction between the big hydrophilic head group (polyethoxyl) of T80 and perovskite, would form many proton-hopping sites.

In contrast to T80, adding Span 80 (S80) as the surfactant in the composite films did not yield a significant result in proton flux as compared to neat mcl-PHA (Table 4.1 and Figure 4.8). This is probably due to the smaller head group of S80 that does not form many proton-hopping sites in the PHA-PV-S80 composite film, thus giving a significantly lower proton flux value than that of T80. The ability of neat mcl-PHA to conduct limited proton transfers is attributed to hydrogen bonding between the hydronium ion (H_3O^+) with carbonyl (C=O) and ether (C-O-C) groups of ester bonds present in the mcl-PHA structure. However, the pH changes reached plateau at 6.3 with neat PHA compared to PHA composite with T80, pH 5.5; lesser number of protons hopping sites present in pristine mcl-PHA is hypothesized to be responsible for the observation made.

The proton flux data as a function of time was fitted using an exponential growth function in order to determine the apparent rate constant, *k*', of the proton flux process. The data range applied for the non-linear regression starts from the beginning of the flux until its maximum i.e., just before it reaches a plateau.

The parameter *k*' also incorporates the partitioning and mass transfer effects of the process. It is interesting to note that the *k*' values for Nafion and neat PHA membranes are comparable or higher than the fabricated composite membranes studied (Table 4.1). In contrast, all composite membranes showed similar or much higher proton flux i.e., up to 4.5 ×. At this point, it is hypothesized that the presence of surfactant and/or perovskite in the composite membranes promoted the partitioning of water molecules, hence protons, on the membrane surface, which subsequently facilitate the proton flux across its thickness to the opposite side. Thus, despite the lower *k*' values for the composite membranes, the proton flux is augmented by the compositing of surfactant and perovskite into the PHA matrix.

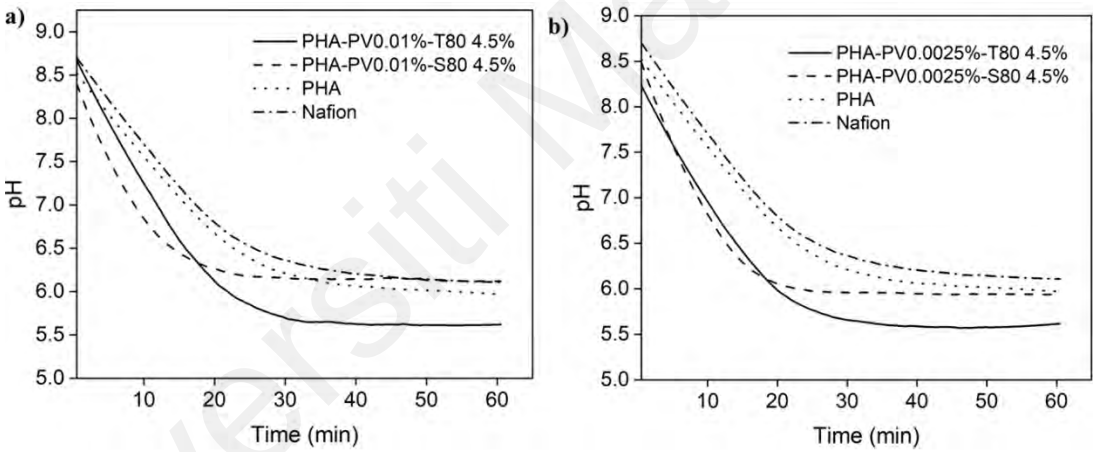

Figure 4.8: pH changes profiles by using neat PHA, Nafion and different PHA composites as proton exchange membranes in ultrapure water medium. PHA composites with (a) high and (b) low perovskite amounts were tested.

Table 4.1: Proton flux and *k'* values of PHA-PV-T80 and PHA-PV-S80 composites in ultrapure water (standard deviation < 5 %)

Film composites	Proton flux ($\times 10^{-4}$ mol.min^{-1}.cm^{-2})	Apparent rate constant, *k'* (min^{-1})
PHA-PV0.01%-T80 4.5% (Tween 80)	4.61	0.060
PHA-PV0.01% -S80 4.5% (Span 80)	1.25	0.011
PHA-PV0.0025% -T80 4.5% (Tween 80)	4.60	0.072
PHA-PV0.0025% -S80 4.5% (Span 80)	1.20	0.014
PHA	1.03	0.074
Nafion	1.22	0.107

From Figure 4.9, it can be observed that much higher proton fluxes were obtained for each investigated membrane when tap water was used as the medium compared to ultrapure water. It is also clear that PHA-PV-T80 composites are transferring protons more efficiently than the rest. While it is unexceptional for the observed *k*' values to differ between ultrapure water and tap water environment, it is interesting that all the studied membranes showed significantly low *k*' values in tap water except for two i.e., PHA-PV0.01%-T80 4.5% and PHA-PV0.01%-S80 4.5%, which exhibited comparable *k*' (Table 4.2). However, the proton flux for the former is significantly higher than the latter, with the sole difference between them is the chemical identity of the surfactant used. It is clear that Tween 80 exhibits superior partitioning properties for water molecules compared to Span 80 due to the reason explained earlier. It is also noteworthy that despite four-fold less perovskite amount in the composite membrane, and much lower *k*' value presumably due to less perovskite, PHA-PV0.0025%-T80 4.5% showed comparable proton flux to PHA-PV0.01%-T80 4.5%, which suggested that the water partitioning effect afforded by the incorporation of surfactant into the composite membrane plays a greater role in achieving a high proton flux. Finally, the generally low *k*' observed in tap water is attributed to the surface polarization effects from the different cations present in the tap water, which curtails proton flux.

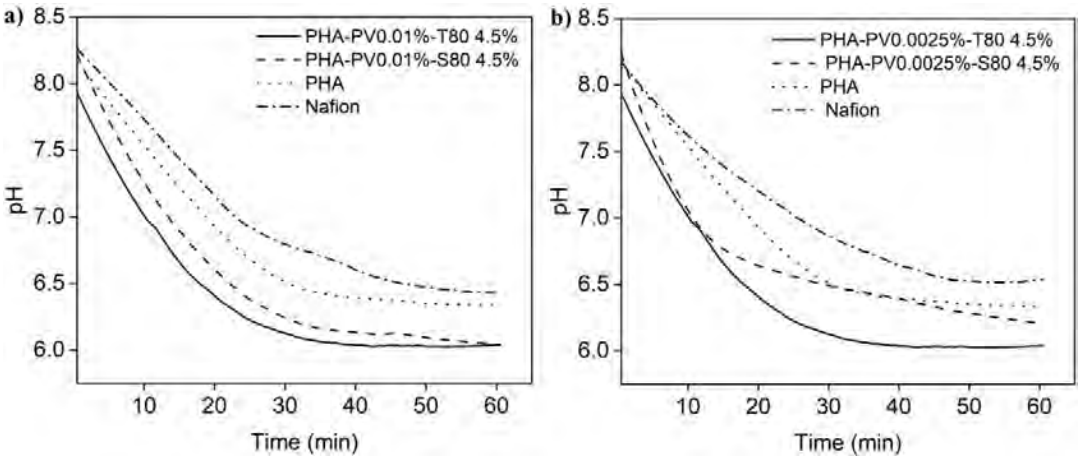

Figure 4.9: pH changes profiles by using neat PHA, Nafion and different PHA composites as proton exchange membranes in tap water medium. PHA composites with (a) high and (b) low perovskite amounts were tested.

Table 4.2: Proton flux and *k'* values of PHA-PV-T80 and PHA-PV-S80 composites in tap water (standard deviation < 5 %)

Film composites	Proton flux ($\times 10^{-5}$ mol.min^{-1}.cm^{-2})	Apparent rate constant, *k'* (min^{-1})
PHA-PV0.01%-T80 4.5% (Tween 80)	9.85	0.044
PHA-PV0.01% -S80 4.5% (Span 80)	6.42	0.041
PHA-PV0.0025% -T80 4.5% (Tween 80)	8.82	0.002
PHA-PV0.0025% -S80 4.5% (Span 80)	4.21	0.002
PHA	3.12	0.006
Nafion	2.23	0.008

Figure 4.10 shows the efficiency of proton transfer through PHA-PV-T80 composite films in ultrapure water. Meanwhile, the proton flux and *k*' for different types of freshly prepared films of PHA-PV-T80 are shown in Table 4.3. From the values of *k*', increasing the quantity of T80 in the composite preparations, except for the composite preparation with highest Tween 80 composition at 4.5 %, resulted in an elevation of the proton flux. However, the augmentation of the perovskite quantity yielded negligible variation in the proton flux. The observation highlights the significance of T80 within the context of the PHA proton exchange membrane as previously discussed. PHA composite with the highest concentration of surfactant (T80) exhibited the most efficient proton transfer attributed to greater number of interaction sites for hydrogen bonding on hydrophilic head group (polyethoxyl) of T80 and perovskite.

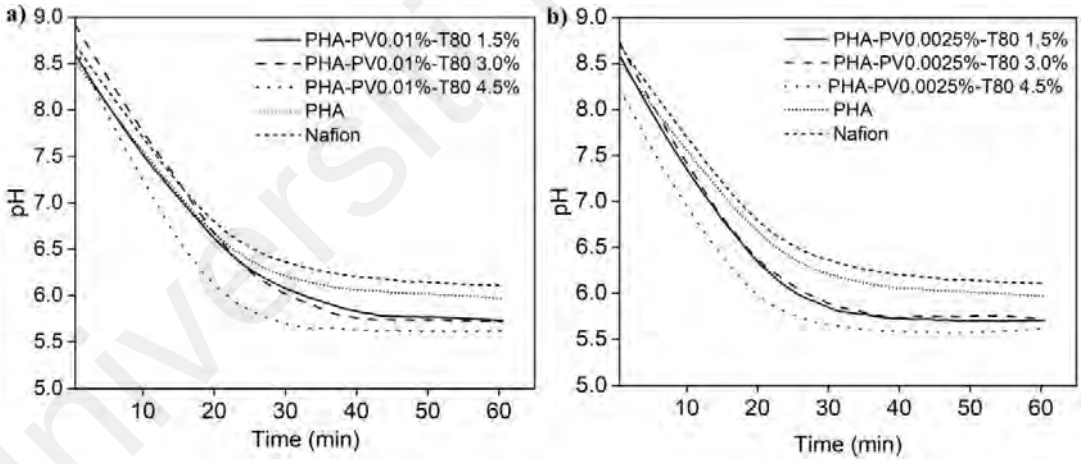

Figure 4.10: pH changes profiles by using PHA-PV-T80 composites as proton exchange membrane in ultrapure water medium. PHA composites with (a) high and (b) low perovskite amounts were tested.

Table 4.3: Proton flux and *k'* values of PHA-PV-T80 composites (standard deviation < 5 %)

Film composites	Proton flux ($\times 10^{-4}$ mol.min^{-1}.cm^{-2})	Apparent rate constant, *k'* (min^{-1})
PHA-PV0.01%-T80 1.5% (Tween 80)	4.18	0.113
PHA-PV0.01% -T80 3.0% (Tween 80)	4.36	0.121
PHA-PV0.01% -T80 4.5% (Tween 80)	4.65	0.060
PHA-PV0.0025% -T80 1.5% (Tween 80)	3.66	0.053
PHA-PV0.0025% -T80 3.0% (Tween 80)	3.62	0.080
PHA-PV0.0025% -T80 4.5% (Tween 80)	4.61	0.072
PHA	1.03	0.074
Nafion	1.22	0.107

4.7 Possible mechanisms of proton transfer across membrane

Based on the result, proton transfer across the membrane thickness is suggested to be determined by the chemical properties of PHA-PV-T80 membrane. The presence of surfactant (Tween 80) and perovskite ($SrTiO_3$) in the mcl-PHA composite membrane increased its hydrophilic properties due to the nature of the surfactant head (polyethoxylated sorbitan) as well as oxygen vacancies found in the perovskite nanoparticles. Therefore, high amounts of water molecules can be adsorbed on and into the composite film layer, aiding the transfer of protons across the membrane thickness.

As illustrated in Figure 4.11, it is hypothesized that proton is transferred across the PHA composite membrane (represented as green arrow) *via* combination of three theorized mechanisms, i.e., Proton hopping, Grotthuss and Vehicular mechanisms;

1) Proton transport could potentially occur between adjacent oxygen of perovskite and ether (C-O-C) group of surfactants. Rotational diffusion and intra-octahedra proton transfer (hopping) in trap region areas are both possible migration paths used by the perovskite to transport protons. Rotating motion of the protons around the oxygen groups is fast, thus proton reorientation occurs at the next oxygen before transfer (Hooshyari *et al.*, 2020).

2) The Grothuss mechanism describes proton hopping/movement *via* a network of hydrogen bonding in hydronium ions as the intermediate state like $H_5O_2^+$ (Zundel cation) and $H_9O_4^+$ (Eigen cation) in water molecules, playing the role as proton donor and proton acceptor, respectively, in the proton migration series (Raja K *et al.*, 2019).

3) Vehicular mechanism describes the proton movement in the state of hydronium ions (H_3O^+) within water molecules similar to diffusion (Raja K *et al.*, 2019).

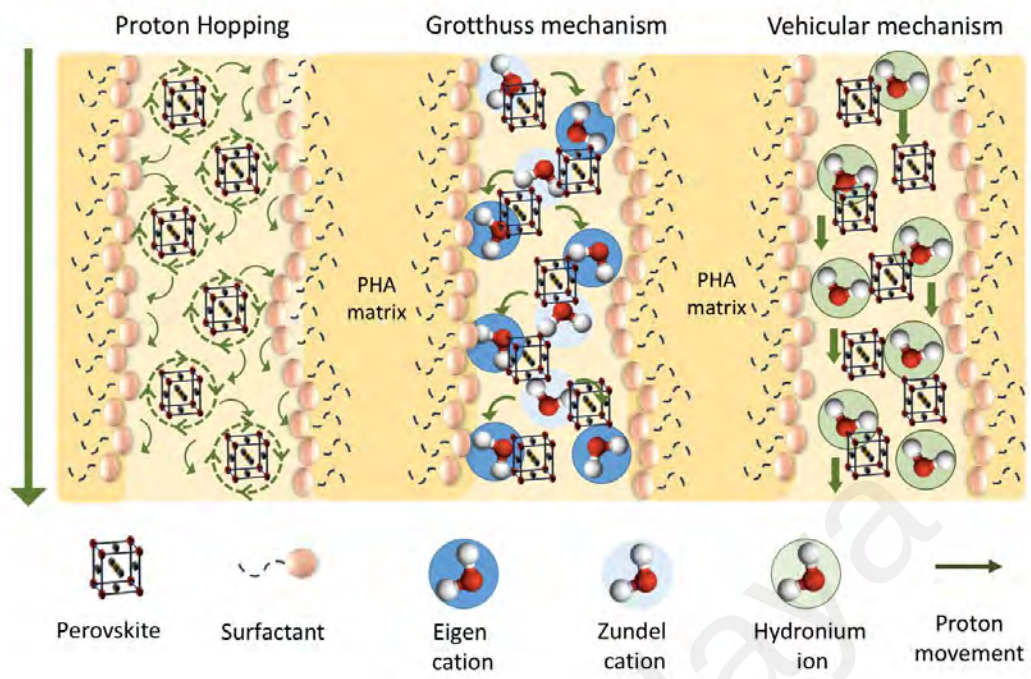

Figure 4.11: Possible mechanisms of proton transport across PHA composite membrane

CHAPTER 5: CONCLUSION

5.1 Conclusion

Medium-chain-length PHA (mcl-PHA), prepared by cultivating *P. putida* BET001 in batch fermentation, was shown to be a good polymer matrix for incorporation of perovskite ($SrTiO_3$) and surfactant (Tween 80). The major constituents of neat mcl-PHA produced are C_8-, C_{10}- and C_{12} monomers. Surface morphology analysis exhibited a homogeneous dispersion of perovskite and surfactant within the matrix of membrane composites. Spectral analysis shows the robust interaction between the PHA matrix, perovskite and surfactant. The degradation temperatures in the PHA-PV-T80 composites were slightly higher than neat mcl-PHA showing improved thermal stability. An additional glass transition temperature was also observed in the composites, hence the membrane alluding to the simultaneous presence of rigidity and flexibility properties. Proton transport analysis of PHA-PV-T80 composites showed that PHA-PV0.01%-T80 4.5% preparation produced the highest flux in comparison to control membranes of neat mcl-PHA and Nafion. It lends strong support that the compositing of perovskite and surfactant within the mcl-PHA matrix improves the transport of proton within the membrane preparation. Compositing surfactant with larger hydrophilic head group in the PHA matrix, as opposed to increasing the perovskite amount, is hypothesized to play a greater role in the partitioning of water molecules on membrane surface, hence facilitating proton flux. The composite may fulfill the need for an alternative membrane material for water purification *via* filtration.

5.2 Recommendation and Future Work

Although the composite showed good selectivity and rapid flux for proton transfer when tested in an aqueous environment, hydrophilicity of polymer is also increased hence the possibility for rapid biodegradation to occur. Future work should consider the appropriate proportion between hydrophilicity and susceptibility to degradation by employing graft copolymerization to combine PHA with methyl acrylate to produce a stronger membrane.

Moreover, proton flux analysis was investigated at ambient conditions for all membrane composites tested in the study. In depth future studies should carry out analysis in different conditions such as elevated temperature to gain understanding regarding the factors that affect the performance of proton flux within the membrane composites.

REFERENCES

Abdel-Fatah, M. A. (2018). Nanofiltration systems and applications in wastewater treatment: review article. *Ain Shams Engineering Journal*, *9*(4), 3077–3092.

Ahmad, A., & Azam, T. (2019). Water Purification Technologies. In A. M. Grumezescu & A. M. Holban (Eds.), *Bottled and packaged water* (pp. 83–120). Cambridge, UK: Woodhead Publishing.

Alam, M. M., ALOthman, Z. A., Naushad, M., & Aouak, T. (2014). Evaluation of heavy metal kinetics through pyridine based Th(IV) phosphate composite cation exchanger using particle diffusion controlled ion exchange phenomenon. *Journal of Industrial and Engineering Chemistry*, *20*(2), 705–709.

Annuar, M. S. M., Tan, I. K. P., Ibrahim, S., & Ramachandran, K. B. (2007). Production of medium-chain-length poly(3-hydroxyalkanoates) from crude fatty acids mixture by Pseudomonas putida. *Food and Bioproducts Processing*, *85*(2), 104–119.

Ansari, N. F., Annuar, M. S. M., & Murphy, B. P. (2017). A porous medium-chain-length poly(3-hydroxyalkanoates)/hydroxyapatite composite as scaffold for bone tissue engineering. *Engineering in Life Sciences*, *17*(4), 420–429.

Azrina, A., Khoo, H. E., Idris, M. A., Amin, I., & Razman, M. R. (2011). Major inorganic elements in tap water samples in Peninsular Malaysia. *Malaysian Journal of Nutrition*, *17*(2), 271–276.

Bhalla, A. S., Guo, R., & Roy, R. (2000). The perovskite structure—a review of its role in ceramic science and technology. *Materials Research Innovations*, *4*(1), 3–26.

Bolisetty, S., Peydayesh, M., & Mezzenga, R. (2019). Sustainable technologies for water purification from heavy metals: review and analysis. *Chemical Society Reviews*, *48*(2), 463–487.

Browne, M. A., Dissanayake, A., Galloway, T. S., Lowe, D. M., & Thompson, R. C. (2008). Ingested microscopic plastic translocates to the circulatory system of the Mussel,Mytilus edulis(L.). *Environmental Science & Technology*, *42*(13), 5026–5031.

Chen, J. P., Mou, H., Wang, L. K., & Matsuura, T. (2006). Membrane filtration. In L. K. Wang, Y. T. Hung, & N. K. Shammas (Eds.), *Advanced Physicochemical Treatment Processes* (pp. 203–259). Totowa, NJ: Humana Press.

Chodák, I. (2008). Chapter 22 - Polyhydroxyalkanoates: origin, properties and applications. In M. N. Belgacem & A. Gandini (Eds.), *Monomers, Polymers and Composites from Renewable Resources* (pp. 451–477). Oxford, UK: Elsevier.

Choi, Y. J., Ahn, Y., Kang, M. S., Jun, H. K., Kim, I. S., & Moon, S. H. (2003). Preparation and characterization of acrylic acid-treated bacterial cellulose cation-exchange membrane. *Journal of Chemical Technology & Biotechnology*, *79*(1), 79–84.

Choudhary, M., Peter, C. N., Shukla, S. K., Govender, P. P., Joshi, G. P., & Wang, R. (2020). Environmental issues: a challenge for wastewater treatment. In M. Naushad & E. Lichtfouse (Eds.), *Green Materials for Wastewater Treatment* (pp. 1–12). Cham, SWTZ: Springer.

Chung, A. L., Jin, H. L., Huang, L. J., Ye, H. M., Chen, J. C., Wu, Q., & Chen, G. Q. (2011). Biosynthesis and characterization of poly(3-hydroxydodecanoate) by β-oxidation inhibited mutant of Pseudomonas entomophilaL48. *Biomacromolecules*, *12*(10), 3559–3566.

Dai, H., Zhong, Y., Wu, X., Hu, R., Wang, L., Zhang, Y., Fan, G., Hu, X., Li, J., & Yang, Z. (2018). Synthesis of perovskite-type $SrTiO_3$ nanoparticles for sensitive electrochemical biosensing applications. *Journal of Electroanalytical Chemistry*, *810*, 95–99.

Davidson, J., & Summerfelt, S. T. (2005). Solids removal from a coldwater recirculating system—comparison of a swirl separator and a radial-flow settler. *Aquacultural Engineering*, *33*(1), 47–61.

de Smet, M. J., Eggink, G., Witholt, B., Kingma, J., & Wynberg, H. (1983). Characterization of intracellular inclusions formed by Pseudomonas oleovorans during growth on octane. *Journal of Bacteriology*, *154*(2), 870–878.

Deshmukh, V. V., Ravikumar, C. R., Kumar, M. R. A., Ghotekar, S., Kumar, A. N., Jahagirdar, A. A., & Murthy, H. C. A. (2021). Structure, morphology and electrochemical properties of $SrTiO_3$ perovskite: photocatalytic and supercapacitor applications. *Environmental Chemistry and Ecotoxicology*, *3*, 241–248.

Fan, Z., Wang, Z., Duan, M., Wang, J., & Wang, S. (2008). Preparation and characterization of polyaniline/polysulfone nanocomposite ultrafiltration membrane. *Journal of Membrane Science*, *310*(1-2), 402–408.

Fan, Z., Wang, Z., Sun, N., Wang, J., & Wang, S. (2008). Performance improvement of polysulfone ultrafiltration membrane by blending with polyaniline nanofibers. *Journal of Membrane Science*, *320*(1-2), 363–371

Francis, L. (2011). *Biosynthesis of polyhydroxyalkanoates and their medical applications* (Doctoral dissertation).
Retrieved from http://www.westminster.ac.uk/research/westminsterresearch

Grabowska, E. (2016). Selected perovskite oxides: Characterization, preparation and photocatalytic properties—a review. *Applied Catalysis B: Environmental*, *186*, 97–126.

Gumel, A. M., & Annuar, M. S. M. (2014). Poly-3-hydroxyalkanoates-*co*-polyethylene glycol methacrylate copolymers for pH responsive and shape memory hydrogel. *Journal of Applied Polymer Science*, *131*(23), 1-11.

Gumel, A. M., Annuar, M. S. M., & Heidelberg, T. (2012). Biosynthesis and characterization of polyhydroxyalkanoates copolymers produced by Pseudomonas putida BET001 isolated from palm oil mill effluent. *PLOS ONE*, *7*(9), 1-8.

Gumel, A. M., Annuar, M. S., & Heidelberg, T. (2014). Growth kinetics, effect of carbon substrate in biosynthesis of mcl-PHA by Pseudomonas putida BET001. *Brazilian Journal of Microbiology*, *45*(2), 427–438.

Guo, W., Duan, J., Geng, W., Feng, J., Wang, S., & Song, C. (2013). Comparison of medium-chain-length polyhydroxyalkanoates synthases from Pseudomonas mendocina NK-01 with the same substrate specificity. *Microbiological Research*, *168*(4), 231–237.

Hackett, E., Manias, E., & Giannelis, E. P. (2000). Computer simulation studies of PEO/layer silicate nanocomposites. *Chemistry of Materials*, *12*(8), 2161–2167.

Harewood, A. J. T., Popuri, S. R., Cadogan, E. I., Lee, C. H., & Wang, C. C. (2017). Bioelectricity generation from brewery wastewater in a microbial fuel cell using chitosan/biodegradable copolymer membrane. *International Journal of Environmental Science and Technology*, *14*(7), 1535–1550.

Hazer, B., & Steinbüchel, A. (2007). Increased diversification of polyhydroxyalkanoates by modification reactions for industrial and medical applications. *Applied Microbiology and Biotechnology*, *74*(1), 1–12.

Hernández-Flores, G., Poggi-Varaldo, H. M., & Solorza-Feria, O. (2016). Comparison of alternative membranes to replace high cost Nafion ones in microbial fuel cells. *International Journal of Hydrogen Energy*, *41*(48), 23354–23362.

Hindatu, Y., Annuar, M. S. M., Subramaniam, R., & Gumel, A. M. (2017). Medium-chain-length poly-3-hydroxyalkanoates-carbon nanotubes composite anode enhances the performance of microbial fuel cell. *Bioprocess and Biosystems Engineering*, *40*(6), 919–928.

Hooshyari, K., Heydari, S., Javanbakht, M., Beydaghi, H., & Enhessari, M. (2020). Fabrication and performance evaluation of new nanocomposite membranes based on sulfonated poly(phthalazinone ether ketone) for PEM fuel cells. *RSC Advances*, *10*(5), 2709–2721.

Hooshyari, K., Javanbakht, M., Shabanikia, A., & Enhessari, M. (2015). Fabrication $BaZrO_3$/PBI-based nanocomposite as a new proton conducting membrane for high temperature proton exchange membrane fuel cells. *Journal of Power Sources*, *276*, 62–72.

Hossain, S., Abdalla, A. M., Jamain, S. N. B., Zaini, J. H., & Azad, A. K. (2017). A review on proton conducting electrolytes for clean energy and intermediate temperature-solid oxide fuel cells. *Renewable and Sustainable Energy Reviews*, *79*, 750–764.

Huang, C., Zhao, G., Song, Y., Xie, C., Zhang, S., & Li, X. (2022). Preparation of novel biodegradable cellulose nanocrystal proton exchange membranes for direct methanol fuel-cell applications. *ACS Sustainable Chemistry & Engineering*, *10*(17), 5559–5568.

Hube, S., Eskafi, M., Hrafnkelsdóttir, K. F., Bjarnadóttir, B., Bjarnadóttir, M. Á., Axelsdóttir, S., & Wu, B. (2020). Direct membrane filtration for wastewater treatment and resource recovery: a review. *Science of the Total Environment*, *710*, 1-22.

Ishak, K. A., Annuar, M. S. M., Heidelberg, T., & Gumel, A. M. (2016). Ultrasound-assisted rapid extraction of bacterial intracellular medium-chain-length poly(3-hydroxyalkanoates) (mcl-PHAs) in medium mixture of solvent/marginal non-solvent. *Arabian Journal for Science and Engineering*, *41*(1), 33–44.

Ishak, K. A., Safian, N. A. M., & Annuar, M. S. M. (2022). Ecofriendly zinc oxide-decorated poly-3-hydroxyalkanoate—graft—poly-methyl acrylate copolymer film for photocatalysis-mediated water treatment. *Journal of Polymers and the Environment*, *30*(4), 1662–1672.

Jenner, L. C., Rotchell, J. M., Bennett, R. T., Cowen, M., Tentzeris, V., & Sadofsky, L. R. (2022). Detection of microplastics in human lung tissue using μFTIR spectroscopy. *Science of the Total Environment*, *831*, 1-10.

Jiang, X., Ramsay, J. A., & Ramsay, B. A. (2006). Acetone extraction of mcl-PHA from Pseudomonas putida KT2440. *Journal of Microbiological Methods*, *67*(2), 212–219.

Kannan, B. R., Kalidhasan, S., Kumar, A. S. K., Rajesh, N., & Venkataraman, B. H. (2014). An integrated use of biopolymer-ceramic composites towards capacitor and environmental application. *Polymer-Plastics Technology and Engineering*, *53*(6), 626–630.

Klaytae, T., Panthong, P., & Thountom, S. (2013). Preparation of nanocrystalline $SrTiO_3$ powder by sol–gel combustion method. *Ceramics International*, *39*, S405–S408.

Kume, G., Gallotti, M., & Nunes, G. (2008). Review on anionic/cationic surfactant mixtures. *Journal of Surfactants and Detergents*, *11*(1), 1–11.

Kundu, P. P., & Dutta, K. (Eds.). (2018). *Progress and recent trends in microbial fuel cells*. Oxford, UK: Elsevier.

Lageveen, R. G., Huisman, G. W., Preusting, H., Ketelaar, P., Eggink, G., & Witholt, B. (1988). Formation of polyesters by Pseudomonas oleovorans: Effect of substrates on formation and composition of poly-(*R*)-3-hydroxyalkanoates and poly-(*R*)-3-hydroxyalkenoates. *Applied and Environmental Microbiology*, *54*(12), 2924–2932.

Liu, Q., Luo, G., Zhou, X. R., & Chen, G. Q. (2011). Biosynthesis of poly(3-hydroxydecanoate) and 3-hydroxydodecanoate dominating polyhydroxyalkanoates by β-oxidation pathway inhibited Pseudomonas putida. *Metabolic Engineering*, *13*(1), 11–17.

Madauß, L., Foller, T., Plaß, J., Kumar, P. V., Musso, T., Dunkhorst, K., Joshi, R., & Schleberger, M. (2020). Selective proton transport for hydrogen production using graphene oxide membranes. *Journal of Physical Chemistry Letters*, *11*(21), 9415–9420.

Maximous, N., Nakhla, G., Wan, W., & Wong, K. (2009). Preparation, characterization and performance of Al_2O_3/PES membrane for wastewater filtration. *Journal of Membrane Science*, *341*(1), 67–75.

Mohamed, S. M. D. S., Ishak, K. A., Annuar, M. S. M., & Velayutham, T. S. (2021). Synthesis and characterization of methyl acrylate-copolymerized medium-chain-length poly-3-hydroxyalkanoates. *Journal of Polymers and the Environment*, *29*(9), 3004–3014.

Moradi, M., & Yamini, Y. (2012). Surfactant roles in modern sample preparation techniques: a review. *Journal of Separation Science*, *35*(18), 2319–2340.

Muhr, A., Rechberger, E. M., Salerno, A., Reiterer, A., Malli, K., Strohmeier, K., Schober, S., Mittelbach, M., & Koller, M. (2013). Novel description of mcl-PHA biosynthesis by Pseudomonas chlororaphis from animal-derived waste. *Journal of Biotechnology*, *165*(1), 45–51.

Myers, D. (2020). *Surfactant science and technology* (4th ed.). Hoboken, NJ: John Wiley & Sons.

Nomura, C. T., & Taguchi, S. (2007). PHA synthase engineering toward superbiocatalysts for custom-made biopolymers. *Applied Microbiology and Biotechnology*, *73*(5), 969–979.

Ochowiak, M., Matuszak, M., Włodarczak, S., Ancukiewicz, M., & Krupińska, A. (2017). The modified swirl sedimentation tanks for water purification. *Journal of Environmental Management*, *189*, 22–28.

Park, J. S., Song, J. H., Yeon, K. H., & Moon, S. H. (2007). Removal of hardness ions from tap water using electromembrane processes. *Desalination*, *202*(1), 1–8.

Peighambardoust, S. J., Rowshanzamir, S., & Amjadi, M. (2010). Review of the proton exchange membranes for fuel cell applications. *International Journal of Hydrogen Energy*, *35*(17), 9349–9384.

Pendergast, M. M., & Hoek, E. M. V. (2011). A review of water treatment membrane nanotechnologies. *Energy & Environmental Science*, *4*(6), 1946-1971.

Pramod, K., Suneesh, C. V., Shanavas, S., Ansari, S. H., & Ali, J. (2015). Unveiling the compatibility of eugenol with formulation excipients by systematic drug-excipient compatibility studies. *Journal of Analytical Science and Technology*, *6*(1), 34-47.

Rai, R., Keshavarz, T., Roether, J. A., Boccaccini, A. R., & Roy, I. (2011). Medium chain length polyhydroxyalkanoates, promising new biomedical materials for the future. *Materials Science and Engineering: R: Reports*, *72*(3), 29–47.

Raja, K., Raja, P. M., & Ramesh, P. M. (2019). Investigation on SPEEK/PAI/SrTiO3-based nanocomposite membrane for high-temperature proton exchange membrane fuel cells. *Ionics*, *25*(11), 5177–5188.

Ray, S. S., & Bousmina, M. (2005). Biodegradable polymers and their layered silicate nanocomposites: in greening the 21st century materials world. *Progress in Materials Science*, *50*(8), 962–1079.

Ruiz, A. I., Darder, M., Aranda, P., Jimenez, R., Damme, H. V., & Ruiz-Hitzky, E. (2006). Bio-nanocomposites by assembling of gelatin and layered perovskite mixed oxides. *Journal of Nanoscience and Nanotechnology*, *6*(6), 1602–1610.

Sahani, S., Roy, T., & Sharma, Y. C. (2020). Studies on fast and green biodiesel production from an indigenous nonedible Indian feedstock using single phase strontium titanate catalyst. *Energy Conversion and Management*, *203*, 1-20.

Samaniego, A. J., & Espiritu, R. (2022). Prospects on utilization of biopolymer materials for ion exchange membranes in fuel cells. *Green Chemistry Letters and Reviews*, *15*(1), 253–275.

Selvakumar, K., Rajendran, S., & Prabhu, M. R. (2019). Influence of barium zirconate on SPEEK-based polymer electrolytes for PEM fuel cell applications. *Ionics*, *25*(5), 2243–2253.

Shariatinia, Z., & Karimzadeh, Z. (2024). Perovskite oxides as efficient bioactive inorganic materials in tissue engineering: a review. *Materials Today Chemistry*, *35*, 1-42.

Shoshaa, R., Ashfaq, M. Y., & Al-Ghouti, M. A. (2023). Recent developments in ultrafiltration membrane technology for the removal of potentially toxic elements, and enhanced antifouling performance: a review. *Environmental Technology and Innovation*, *31*, 1-20.

Shrivastava, A. (2018). *Introduction to Plastics Engineering*. Oxford, UK: Elsevier.

Sirajudeen, A. A. O., Annuar, M. S. M., Ishak, K. A., Yusuf, H., & Subramaniam, R. (2021). Innovative application of biopolymer composite as proton exchange membrane in microbial fuel cell utilizing real wastewater for electricity generation. *Journal of Cleaner Production*, *278*, 1-10.

Song, J. H., Jeon, C. O., Choi, M. H., Yoon, S. C., & Park, W. (2008). Polyhydroxyalkanoate (PHA) production using waste vegetable oil by Pseudomonas sp strain DR2. *Journal of Microbiology and Biotechnology*, *18*(8), 1408–1415.

Strathmann, H. (2010). Chapter 6 Ion-exchange membrane processes in water treatment. In I. C. Escobar & A. I. Schäfer (Eds.), *Sustainable Water for the Future: Water Recycling versus Desalination* (pp. 141–199). Oxford, UK: Elsevier.

Sunarso, J., Hashim, S. S., Zhu, N., & Zhou, W. (2017). Perovskite oxides applications in high temperature oxygen separation, solid oxide fuel cell and membrane reactor: a review. *Progress in Energy and Combustion Science*, *61*, 57–77.

Tao, Z., Yan, L., Qiao, J., Wang, B., Zhang, L., & Zhang, J. (2015). A review of advanced proton-conducting materials for hydrogen separation. *Progress in Materials Science*, *74*, 1–50.

Tematio, C., Bassas-Galia, M., Fosso, N., Gaillard, V., Mathieu, M., Zinn, M., … Schintke, S. (2017). Design and characterization of conductive biopolymer nanocomposite electrodes for medical applications. *Materials Science Forum*, *879*, 1921–1926.

VanderHart, D. L., Asano, A., & Gilman, J. W. (2001). NMR measurements related to clay-dispersion quality and organic-modifier stability in Nylon-6/Clay nanocomposites. *Macromolecules*, *34*(12), 3819–3822.

Voorhoeve, R. J. H., Johnson, D. W., Remeika, J. P., & Gallagher, P. K. (1977). Perovskite oxides: materials science in catalysis. *Science*, *195*(4281), 827–833.

Vörösmarty, C. J., McIntyre, P. B., Gessner, M. O., Dudgeon, D., Prusevich, A., Green, P., … Davies, P. M. (2010). Global threats to human water security and river biodiversity. *Nature*, *467*(7315), 555–561.

Walkowiak-Kulikowska, J., Wolska, J., & Koroniak, H. (2017). Polymers application in proton exchange membranes for fuel cells (PEMFCs). *Physical Sciences Reviews*, *2*(8), 1-34.

Wang, B., Shang, J., Zhao, Y., Zhong, S., & Cui, X. (2019). Fabrication of functionalized nanosilicone particles-doped biodegradable eco-friendly proton exchange membranes. *Journal of Materials Science*, *54*(23), 14504–14514.

Xu, H. F., Wang, X., Shao, Z. G., & Hsing, I. M. (2002). Recycling and regeneration of used perfluorosulfonic membranes for polymer electrolyte fuel cells. *Journal of Applied Electrochemistry*, *32*(12), 1337–1340.

Yan, L., Li, Y. S., & Xiang, C. B. (2005). Preparation of poly(vinylidene fluoride)(PVDF) ultrafiltration membrane modified by nano-sized alumina (Al_2O_3) and its antifouling research. *Polymer*, *46*(18), 7701–7706.

Yao, H., Wu, L. P., & Chen, G. Q. (2019). Synthesis and characterization of electroconductive PHA- graft-graphene nanocomposites. *Biomacromolecules*, *20*(2), 645–652.

Yusuf, H., Annuar, M. S. M., Subramaniam, R., & Gumel, A. M. (2019). Amphiphilic biopolyester-carbon nanotube anode enhances electrochemical activities of microbial fuel cell. *Chemical Engineering & Technology*, *42*(3), 566–574.